cells

MDPI

Article

Cockayne Syndrome Patient iPSC-Derived Brain Organoids and Neurospheres Show Early Transcriptional Dysregulation of Biological Processes Associated with Brain Development and Metabolism

Leon-Phillip Szepanowski [1,2], Wasco Wruck [1], Julia Kapr [2], Andrea Rossi [2], Ellen Fritsche [2], Jean Krutmann [2] and James Adjaye [1,3,*]

[1] Institute for Stem Cell Research and Regenerative Medicine, University Hospital Düsseldorf, Moorenstrasse 5, D-40225 Duesseldorf, Germany; leon-phillip.szepanowski@iuf-duesseldorf.de (L.-P.S.)
[2] IUF—Leibniz Research Institute for Environmental Medicine, Auf'm Hennekamp 50, D-40225 Duesseldorf, Germany
[3] Zayed Centre for Research into Rare Diseases in Children (ZCR), University College London (UCL)—EGA Institute for Women's Health, 20 Guilford Street, London WC1N 1DZ, UK
* Correspondence: james.adjaye@med.uni-duesseldorf.de

Abstract: Cockayne syndrome (CS) is a rare hereditary autosomal recessive disorder primarily caused by mutations in Cockayne syndrome protein A (CSA) or B (CSB). While many of the functions of CSB have been at least partially elucidated, little is known about the actual developmental dysregulation in this devasting disorder. Of particular interest is the regulation of cerebral development as the most debilitating symptoms are of neurological nature. We generated neurospheres and cerebral organoids utilizing Cockayne syndrome B protein (CSB)-deficient induced pluripotent stem cells derived from two patients with distinct severity levels of CS and healthy controls. The transcriptome of both developmental timepoints was explored using RNA-Seq and bioinformatic analysis to identify dysregulated biological processes common to both patients with CS in comparison to the control. CSB-deficient neurospheres displayed upregulation of the VEGFA-VEGFR2 signalling pathway, vesicle-mediated transport and head development. CSB-deficient cerebral organoids exhibited downregulation of brain development, neuron projection development and synaptic signalling. We further identified the upregulation of steroid biosynthesis as common to both timepoints, in particular the upregulation of the cholesterol biosynthesis branch. Our results provide insights into the neurodevelopmental dysregulation in patients with CS and strengthen the theory that CS is not only a neurodegenerative but also a neurodevelopmental disorder.

Keywords: Cockayne syndrome; brain organoids; RNA-Seq; brain development; steroid biosynthesis

Citation: Szepanowski, L.-P.; Wruck, W.; Kapr, J.; Rossi, A.; Fritsche, E.; Krutmann, J.; Adjaye, J. Cockayne Syndrome Patient iPSC-Derived Brain Organoids and Neurospheres Show Early Transcriptional Dysregulation of Biological Processes Associated with Brain Development and Metabolism. *Cells* **2024**, *13*, 591. https://doi.org/10.3390/cells13070591

Received: 29 February 2024
Revised: 24 March 2024
Accepted: 26 March 2024
Published: 28 March 2024

Copyright: © 2024 by the authors. Licensee MDPI, Basel, Switzerland. This article is an open access article distributed under the terms and conditions of the Creative Commons Attribution (CC BY) license (https://creativecommons.org/licenses/by/4.0/).

1. Introduction

Cockayne syndrome (CS), first described by Edward Alfred Cockayne in 1936 [1], is a rare hereditary autosomal recessive disorder with a prevalence of 2.5 in 1 million births and no apparent overrepresentation in any specific population [2]. The median life expectancy of patients with CS is 12 years, but the time of death spans from neonatal to 55 years [2,3]. As a disease, CS is characterized by severe photosensitivity, failure to thrive, cachectic dwarfism, segmental progeria, vasculopathy, cataracts, dental caries and progressive multisystem degeneration. CS is also known for its various neurological afflictions like intellectual disability, sensorineural hearing loss, progressive microcephaly, cerebellar

hypoplasia, dys- and hypomyelination, dystrophic mineralization of neurons and vessels and segmental demyelinating peripheral neuropathy [4,5].

The two main mutated genes in patients with CS are excision repair cross-complementing protein group 6 ERCC6 (Cockayne syndrome B protein, CSB), which two of three patients exhibit a mutation in, and ERCC8 (Cockayne syndrome A protein, CSA), which comprise the remaining third [4].

The CSB protein is a crucial part of the transcription-coupled nucleotide excision repair mechanism (TC-NER), where it detects the DNA lesion-stalled RNA polymerase II (RNAPII) and initiates the repair process [6]. However, while the dysfunction of repair processes is associated with neurodegenerative diseases [7], loss of this repair mechanism cannot entirely explain the symptoms associated with patients with CS.

Additionally to its function in the TC-NER, CSB has been implicated as enhancing the efficacy of the base excision repair and mitochondrial base excision repair mechanism [8–10], is involved in the repair of double-strand breaks [11,12] and has been implicated in enhancing inter-strand crosslinks repair [13,14]. CSB has also been shown to be involved in transcription regulation. CSB-deficient cells show up to 50% reduced transcription and dysregulation of thousands of genes [15,16].

All these characteristics of CSB have been investigated employing mainly dermal fibroblasts of various patients with CS, Chinese hamster ovary- and mouse model-derived primary cells. Monotypic cell lines are typically well suited for initial gene function analyses and structure–function relationship studies but cannot fully illustrate the impact of a versatile protein such as CSB with multi-system manifestations. In 1997, the first mouse model of CS was described [17], enabling the investigation of primary cells of impacted tissues and whole organisms studies. Since then, mouse models of all CS-associated genes, *CSB*, *CSA*, *XPB*, *XPD* and *XPG*, have been established [18–22]. CS mouse models (except for *XPG*) generally exert a mild CS phenotype with reduced bodyweight, UV-sensitivity, mild neurodegenerative changes and a surprising increase in skin tumorigenesis, a symptom not found in human patients with CS. For the modelling of severe CS, CSA- or CSB-deficient mice can be crossed with mice lacking in other genes of the TC-NER machinery, e.g., *XPA* or *XPC* [19,23].

However, the discrepancy in the function of CS proteins and the need to combine two mutations to replicate specific characteristics emphasize the need for humanized models. The advent of induced pluripotent stem cells (iPSCs) enabled investigators to develop reliable human disease models to study the effects of mutations on human tissues. Several neurodegenerative and mental disorders e.g., Alzheimer, Parkinson's disease, schizophrenia and autism, have been the focal point of stem cell-based neurological research. However, this rare disease has only been subject of a few iPSC-based studies [24–29]. Some of these studies concentrated on CS patient-derived human dermal fibroblasts or SH-SY5Y cells and only incorporated CSB-deficient iPSC lines for singular experiments. Still, these studies have provided great insight into the transcriptional dysregulation in patients with CS. Several important pathways have been identified to be dysregulated in CS patient iPSC-derived neuronal networks e.g., axonogenesis, action potential of neurons, GH/IGF-1 signalling pathway, synaptic transmission, synaptogenesis and density of synapses [27]. In accordance with these enrichment clusters, a reduced synapse density, a reduced spike number and an altered network synchrony have been identified in iPSC-derived neuronal networks [27]. Two studies also identified dysregulation of miRNAs in CSB-deficient iPSCs and iPSC-derived neuronal networks [24,27]. A successful rescue attempt via CRISPR/Cas9 has demonstrated that restoration of one of two mutations in heterozygous mutants is sufficient to restore CSB function in CSB-deficient iPSCs and neural and mesenchymal stem cells [28]. Also, pharmacological intervention in iPSC-derived neurons has shown that TRKB agonists can increase arborization and neurite numbers in CSB-deficient iPSC-derived neurons [26].

All these studies have used iPSCs or iPSC-derived 2D and 2.5D neuronal models. So far, no one has utilised the approach of self-organising organoids, which better recapitulate the cellular heterogeneity, structure and functions of the primary tissues.

In this study, we sought to shed light on common transcriptional dysregulation associated with early cerebral development in patients with CS. However, as CS is a rare disease, obtaining patient material for reprogramming is difficult. We managed to acquire iPSC lines derived from (i) two individuals with CS and (ii) a healthy control and differentiated them into expandable neural progenitor cells (NPCs) and cerebral organoids (COs). Next, we utilized next-generation sequencing (NGS) to analyse RNA transcription at the NPC stage and after 60 days of CO differentiation. Here, we compared NPCs and COs generated from CS patient-derived iPSCs with each other and an unaffected control. Comparative gene expression analysis revealed the dysregulation of several cellular pathways common between the two individuals. These included enrichment clusters which have been shown to be dysregulated in neurons, such as pathways associated with synaptogenesis, synaptic maintenance, axon guidance and the p53 signalling pathway but also pathways important for brain development and homeostasis, which have not been implicated in CS before. These included, e.g., the VEGFA-VEGFR2 signalling pathway, vesicle-mediated transport, and important metabolic pathways like steroid biosynthesis.

2. Materials and Methods

2.1. iPSC Culture Methods

The iPSC lines derived from patients with CS (CS789 and IUFi001) as well as the control line B4 used in this study have been previously described [30–32].

One clone per iPSC line was used for further investigation. iPSC lines were cultured in mTeSR Plus medium (StemCell Technologies, Vancouver, BC, Canada) supplemented with penicillin/streptomycin (P/S) (Gibco; Thermo Fisher Scientific, Inc., Waltham, MA, USA) on Matrigel-coated six-well plates (Corning, New York, NY, USA). The medium was changed every day, and cells were passaged at 70–80% confluency every 5–7 days using $PBS^{Ca-/Mg-}$ (Life Technologies; Thermo Fisher Scientific, Inc., Waltham, MA, USA) supplemented with 0,5 mM UltraPureTM EDTA (Gibco; Thermo Fisher Scientific, Inc., Waltham, MA, USA).

2.2. Generation of Neurospheres

For the generation of neurospheres, iPSCs were differentiated using a modified version of a protocol previously described in our workgroup [33–36].

Briefly, iPSCs were dissociated using TrypLE Express (Gibco; Thermo Fisher Scientific, Inc., Waltham, MA, USA) and seeded into ultra-low-attachment 96-well plates (NunclonTM SpheraTM, Thermo Fisher Scientific, Inc., Waltham, MA, USA) at 10,000 cells/well with mTeSR medium supplemented with 10 μM Y-27632 (Tocris Bioscience; Biotechne, Minneapolis, MN, USA). Neural induction was commenced at day 2 by replacing the medium with neural induction medium (NIM; 47.5% neurobasal A, 47.5% DMEM/F12, 2% B27 w/o vitamin A, 1% N2 supplement, 1% GlutaMAX, 1% penicillin/streptomycin; all from Gibco) supplemented with 10 μM SB-431542 (Torics Bioscience, Bristol, UK), 5 μM dorsomorphin (Tocris Bioscience) and 10 μM Y-27632. The medium was changed daily, and at day 6, Y-27632 was omitted. At day 8, the spheroids were transferred to poly-ornithine and laminin-coated (both Sigma-Aldrich; Merck KGaA, Darmstadt, Germany) six-well plates containing prewarmed neural differentiation medium (NDM; neurobasal A, 2% B27, 1% N2, 1% GlutaMAX , 1% P/S; all from Gibco) supplemented with 20 ng/mL of EGF and FGF2 (both PeproTech; Thermo Fisher Scientific, Inc., Waltham, MA, USA). The attached spheroids were further cultured in an incubator with 5% CO_2 and 37 °C with daily medium changes. On day 16, the neural rosettes were detached using STEMdiffTM Neural Rosette Selection Reagent (StemCell Technologies, Vancouver, BC, Canada) and transferred to non-adhesive 100 mm dishes containing NIM supplemented with 20 ng/ml

FGF2 and EGF. From day 16 onwards, neurospheres were cultured in a shaking incubator (New Brunswick S41i, Eppendorf, Hamburg, Germany) under continuous agitation (60 rpm) with 5% CO_2 at 37 °C with daily medium change.

2.3. Generation of Organoids

For the generation of cerebral organoids, iPSCs were differentiated as described previously in our workgroup [33,35], with minor modifications. In short, iPSCs were dissociated using TrypLE Express (Gibco; Thermo Fisher Scientific, Inc., Waltham, MA, USA) and seeded into ultra-low-attachment 96-well plates (NunclonTM SpheraTM, Thermo Fisher Scientific, Inc., Waltham, MA, USA) at 10,000 cells/well with mTeSR medium supplemented with 10 µM Y-27632 (Tocris Bioscience; Biotechne, Minneapolis, MN, USA). Neural induction was commenced on day 2 by replacing the medium with neural induction medium (NIM; 47.5% neurobasal A, 47.5% DMEM/F12, 2% B27 w/o vitamin A, 1% N2 supplement, 1% GlutaMAX, 1% penicillin/streptomycin; all from Gibco) supplemented with 10 µM SB-431542 (Tocris Bioscience), 5 µM dorsomorphin (Tocris Bioscience) and 10 µM Y-27632. The medium was changed daily, and on day 6, Y-27632 was omitted. On day 8, the spheroids were transferred to non-adhesive 100 mm dishes containing neural differentiation medium (NDM; neurobasal A, 2% B27, 1% N2, 1% GlutaMAX, 1% P/S, all from Gibco) supplemented with 20 ng/ml of EGF and FGF2 (both PeproTech; Thermo Fisher Scientific, Inc., Waltham, MA, USA). Organoids were further cultured in a shaking incubator (New Brunswick S41i, Eppendorf) under continuous agitation (60 rpm) with 5% CO_2 at 37 °C. The medium was changed daily until day 25. From day 25 to day 40, organoids were cultured in NDM supplemented with 20 ng/mL BDNF and NT-3 (both PeproTech; Thermo Fisher Scientific, Inc., Waltham, MA, USA). The medium was changed every 3 days. From day 40 onwards, the organoids were kept in NDM without further supplements with bi-weekly medium changes.

2.4. Neurosphere/Organoid Sectioning and Immunocytochemistry

Cerebral organoids were fixed in ice-cold 4% paraformaldehyde (PFA) for 1 h at room temperature, washed three times with PBS and dehydrated for 24 h in 30% sucrose/PBS at 4 °C.

Subsequently, the organoids were transferred to cryomolds containing Tissue-Tek OCT Compound 4583 embedding medium (Sakura Finetek, Umkirch, Germany), snap-frozen on liquid nitrogen and stored at −80 °C. The organoids were cut into 10 µm sections using a cryostat (CM1850, Leica, Nussloch, Germany) and captured on Superfrost Plus slides (Thermo Fisher Scientific, Inc., Waltham, MA, USA). For immunocytochemistry, cryosections were permeabilized with 0.5% Triton X-100 in PBS for 10 min and blocked with PBS containing 3% BSA and 0.1% Triton X-100 for 1 h. The samples were then incubated overnight at 4 °C with the following primary antibodies: mouse anti-βIII-tubulin (1:400, Cell Signalling Technologies #4466S, Danvers, MA, USA), rabbit anti-SOX2 (1:400, Cell Signalling Technologies #3579S), guinea pig anti-DCX (1:200, Merck Millipore #AB2253, Darmstadt, Germany), mouse anti-KI67 (1:400, Cell Signalling Technologies #9449S), rabbit anti-cleaved CASP3 (1:400, Cell Signalling Technologies #9664S), rabbit Nestin (1:1000, Merck Sigma-Aldrich #N5413, Darmstadt, Germany), mouse anti-MAP2 (Synaptic Systems, 1:500 #188011, Göttingen, Germany), guinea pig anti-NeuN (1:500, Synaptic Systems #266004), mouse anti-TAU (1:1000, Invitrogen, Thermo Fisher Scientific #MN1000), rabbit anti-S100B (1:100, Abcam #ab52642, Cambridge, UK), goat anti SOX1 (1:200, R&D Systems, Biotechne #AF3369, Minneapolis, MN, USA) and rabbit anti-gH2A.X (1:400, Cell Signalling Technologies #9718S). All antibodies are listed in Supplemental Table S1. The samples were washed three times with room-temperature (RT) PBS. The samples were further incubated with the appropriate secondary antibody conjugated with either Alexa-488, Alexa-555 or Alexa-647 (all 1:500, Invitrogen, Thermo Fisher Scientific) and the nuclear stain Hoechst 33258 (2 ug/mL, Sigma-Aldrich, Merck) for 2 h at RT. The slices were mounted with Fluoromount-G (Southern Biotech, Birmingham, AL, USA) and dried

overnight at room temperature. Fluorescent images were obtained using an LSM 700 microscope (Carl Zeiss, Jena, Germany) and processed using ZEN 2012 software (version 1.1.2.0; Carl Zeiss) and ImageJ (FIJI version 2.14.0/1.54f; National Institutes of Health, Bethesda, MD, USA).

2.5. Image Analysis of Neurosphere and Organoid Histological Sections

Fluorescent images were obtained using an LSM 700 microscope (Carl Zeiss, Jena, Germany) and further analysed using ImageJ (FIJI version 2.14.0/1.54f; National Institutes of Health, Bethesda, MD, USA).

To determine the number of Hoechst-, SOX2-, KI67- and gH2A.X-positive cells, 3–4 random sections were chosen per organoid/neurosphere, and the number of positive nuclei was determined by manual counting. For cleaved CASP3, ImageJ was used to determine the integrated density, area and the background fluorescence of 3–4 random sections per organoid/neurosphere. These values were then used to calculate the corrected total cell fluorescence (CTCF).

2.6. Quantitative Reverse Transcription PCR (RT-qPCR)

Total RNA was extracted from iPSCs, 15–20 pooled day 30 neurospheres and 5–7 pooled day 60 organoids using TRIzol (Invitrogen; Thermo Fisher Scientific Inc., Waltham, MA, USA) and Direct-Zol RNA Mini Prep (Zymo Research, Freiburg, Germany). Extractions were performed according to the manufacturer's protocol. Moreover, 500 ng purified RNA was used for cDNA synthesis using a TaqMan reverse transcription reagent (Applied Biosystems; Thermo Fisher Scientific, Inc., Waltham, MA, USA).

The quantification of transcripts was performed by reverse transcription quantitative PCR (RT-qPCR) using the SYBR® Green RT-PCR assay (Applied Biosystems). Amplification, the detection of specific gene products and quantitative analysis were performed using the ViiA7 sequence detection system (Applied Biosystem). The expression levels were normalized relative to the expression of the housekeeping gene RPLP0 and analysed via the $2^{-\Delta\Delta CT}$ method. RT-qPCR data are depicted as mean values. Primers are listed in Supplemental Table S1.

2.7. Next-Generation Sequencing

Moreover, 1 µg RNA of each sample (n = 1 for each condition; 15–20 pooled day 30 neurospheres and 5–7 pooled day 60 organoids) was subjected to bulk next-generation sequencing (NGS) at BGI Genomics (BGI Group, Shenzhen, China). BGI performed the RNA-Seq (transcriptome) library preparation via the stranded mRNA enrichment method. Sequencing was performed on a DNBSeq PE100 platform with 20 M clean reads per sample.

FPKM (fragments per kilobase per million mapped fragments) and count values aligned by the BGI via the HISAT software (HISAT2 version 2.2.1) [37] to the reference genome GCF_000001405.38_GRCh38.p12 were imported into the R/Bioconductor environment [38]. Genes were considered expressed when the counts value was greater than the threshold of t = 5. Venn diagrams were generated based on expressed genes using the R package VennDiagram [39]. Dendrograms and heatmap were generated via the R methods "heatmap.2" and "hclust" from the R package gplots [40] or the R core functionality using Pearson's correlation as a similarity measure. Gene ontologies (GOs) were analysed via the GOstats R package [41]. KEGG pathways [42–45] were downloaded from the KEGG database in July 2020 and tested for the over-representation of genes via the R-built-in hypergeometric test. Dot plots of the most significantly over-represented pathways or GOs were generated via the R package ggplot2 [46]. Differentially expressed genes between two conditions were determined via the R-built-in Fisher's exact test using the criteria $p < 0.05$ and the ratio >1.5 for upregulation or ratio <2/3 for downregulation.

A comprehensive functional analysis of the clustered GO biological processes and pathways (KEGG pathways, Reactome gene sets, canonical pathways and CORUM) of gene sets based on a previous Venn analysis was performed using Metascape (http://metascape.org, accessed on 27 July 2022 and 3 March 2023) [47].

To identify the developmental age and enriched brain regions in the neurospheres and organoids, NGS datasets associated with foetal brain regions were downloaded from the Allen Brain Atlas (ABA) (https://www.brainspan.org/, accessed on 19 January 2022) [48]. Genes specific for brain regions were extracted from the ABA expression RPKM (reads per kilobase per million mapped reads) data by first filtering only genes with a coefficient of variation (cv) greater than the median cv. Thereafter, for each brain region, the genes greater than the threshold t95 at the mean of the 95 quantiles of all samples were extracted. Heatmaps of enrichment in the ABA were made via the R package GSVA [49] (gene set variation analysis) and represent the GSVA enrichment scores of the dedicated brain regions. Brain regions are abbreviated by the following acronyms: occipital neocortex—Ocx, primary motor sensory cortex (samples)—M1C-S1C, amygdaloid complex—AMY, medial ganglionic eminence—MGE, posterior (caudal) superior temporal cortex (area 22c)—STC, upper (rostral) rhombic lip—URL, caudal ganglionic eminence—CGE, dorsal thalamus— DTH, anterior (rostral) cingulate (medial prefrontal) cortex—MFC, dorsolateral prefrontal cortex—DFC, orbital frontal cortex—OFC, lateral ganglionic eminence—LGE, inferolateral temporal cortex (area TEv, area 20)—ITC, hippocampus (hippocampal formation)—HIP, ventrolateral prefrontal cortex—VFC, and parietal neocortex—PCx.

2.8. Western Blotting

To harvest the total protein, 10–15 neurospheres and 4–6 organoids per cell line were rinsed twice with PBS and then lysed in RIPA buffer (Sigma-Aldrich; Merck KGaA, Darmstadt, Germany) supplemented with a protease inhibitor cocktail and phosphatase inhibitor cocktail (Roche, Mannheim, Germany). The protein content of lysates was quantified using the PierceTM Protein Assay Kit (Thermo Fisher Scientific Inc., Waltham, MA, USA). Furthermore, 20 μg of the protein samples were then heat-denatured and subsequently separated on a 4–12% Bis-Tris gel (Invitrogen; Thermo Fisher Scientific). The separated proteins were then transferred to a 0.45 μm nitrocellulose membrane via wet blotting for 3 h at 300 mA. The membranes were blocked in Tris-buffered saline/0.1% Tween-20 containing 5% skim milk and afterwards stained with the following antibodies: rabbit anti-CSB (1:1000, GeneTex Inc. #GTX104589, Irvine, CA, USA), rabbit anti-SQLE (1:1000, Proteintech #12544-1-AP, Rosemont, IL, USA), mouse anti-p53 (1:1000, Merck OP43) and mouse anti-β-actin (1:4000, Cell Signalling Technologies #4967S). All antibodies are listed in Supplemental Table S1. After incubation, the blots were washed three times with Tris-buffered saline/0.1% Tween-20 and subsequently stained with the appropriate secondary antibodies. Following three washing steps with Tris-buffered saline/0.1% Tween-20, the protein bands were visualized with ECL Western blotting detection reagents (Cytiva, Freiburg, Germany) in a UV chamber. The resulting bands were quantified using greyscale analysis with ImageJ (National Institutes of Health, Bethesda, MD, USA).

3. Results

3.1. Both Control and CSB-iPSCs Efficiently Differentiate into Neural Progenitors

For this project, we utilized two previously established iPSC lines generated from a patient with cerebro-oculo-fascio-skeletal syndrome (CS789), a patient with classical CS (IUFi001), as well as the established control line B4. The CS789 line carries a homozygous p.R683X mutation in exon 10 of the ERCC6 gene, leading to a stop codon and a predicted truncated protein. The IUFi001 line carries a compound mutation, p.K377X in exon 5 and p.R857X in exon 15 of the ERCC6 gene (Supplementary Figure S1) [30–32].

To investigate how CS affects early human neurodevelopment, we implemented our published suspension protocols for neurospheres (NS) (Figure 1A) and cerebral organoids (COs) (Figure 2A) [33,35]. The neurospheres were cultured for 30 days.

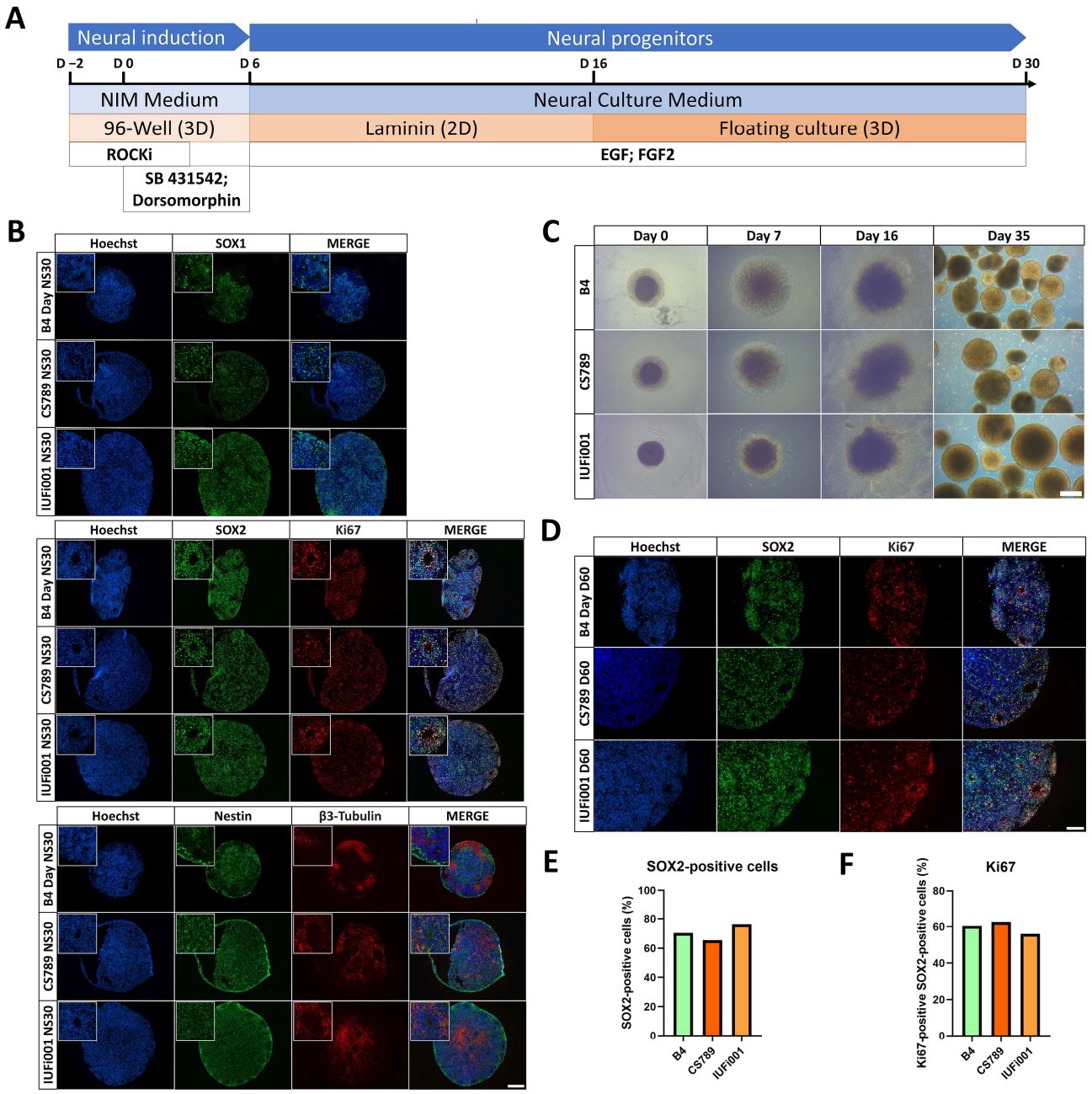

Figure 1. Generation and characterization of CS neurospheres. (**A**) Schematic outline of the protocol to generate iPSC-derived neurospheres. (**B**) Representative immunocytochemistry images of the distribution of cells expressing SOX1, SOX2, Ki67, Nestin and β3-Tubulin. 100× magnification, scale bar 200 µm. (**C**) Representative brightfield images of control and CS neurospheres at day 0, 7, 16 and 35 of differentiation. Scale bar, 200 µm. (**D**) Representative immunocytochemistry images of the distribution of cells expressing SOX2 and Ki67. 200× magnification, scale bar 100 µm. (**E**) Quantification of the SOX2-positive and Hoechst-positive cells in CTRL (B4), CS789 and IUFi001 neurospheres. (**F**) Quantification of the Ki67-positive cells within the SOX2-positive cells in CTRL (B4), CS789 and IUFi001 neurospheres. (**E**,**F**) Approximately ten random fields from three distinct neurospheres were analysed.

By day 30 of differentiation, immunocytochemical analysis revealed that control and CS NS were composed mostly of SRY-box transcription factor 2 (SOX2)+, SRY-box transcription factor 1 (SOX1)+ and Nestin+ neural progenitor cells (NPCs) organized in ventricular zone (VZ)-like structures surrounded by pan-neuronal marker tubulin beta 3 class III (TUBB3)+ early-born neurons (Figure 1B).

During differentiation, all cell lines behaved similarly with regards to attachment, the formation of rosettes and the generation of NS (Figure 1C). The manual assessment of SOX2+ nuclei (Figure 1D,E) and SOX2 and marker of proliferation Ki-67 (Ki-67) double-positive nuclei (Figure 1D,F) did not reveal differences in the number of SOX2+ NPCs and proliferating SOX2+ NPCs between all cell lines.

By comparing the B4, CS789 and IUFi001 NS RNA-Seq datasets with transcriptional datasets from the Allen Brain Atlas, we attempted to determine the developmental age of the NS (Supplementary Figure S2A) as described previously [33,50]. We observed that the transcriptomes of our day 30 NS are equivalent to 8–9 weeks post-conception foetal brains (Supplementary Figure S2B).

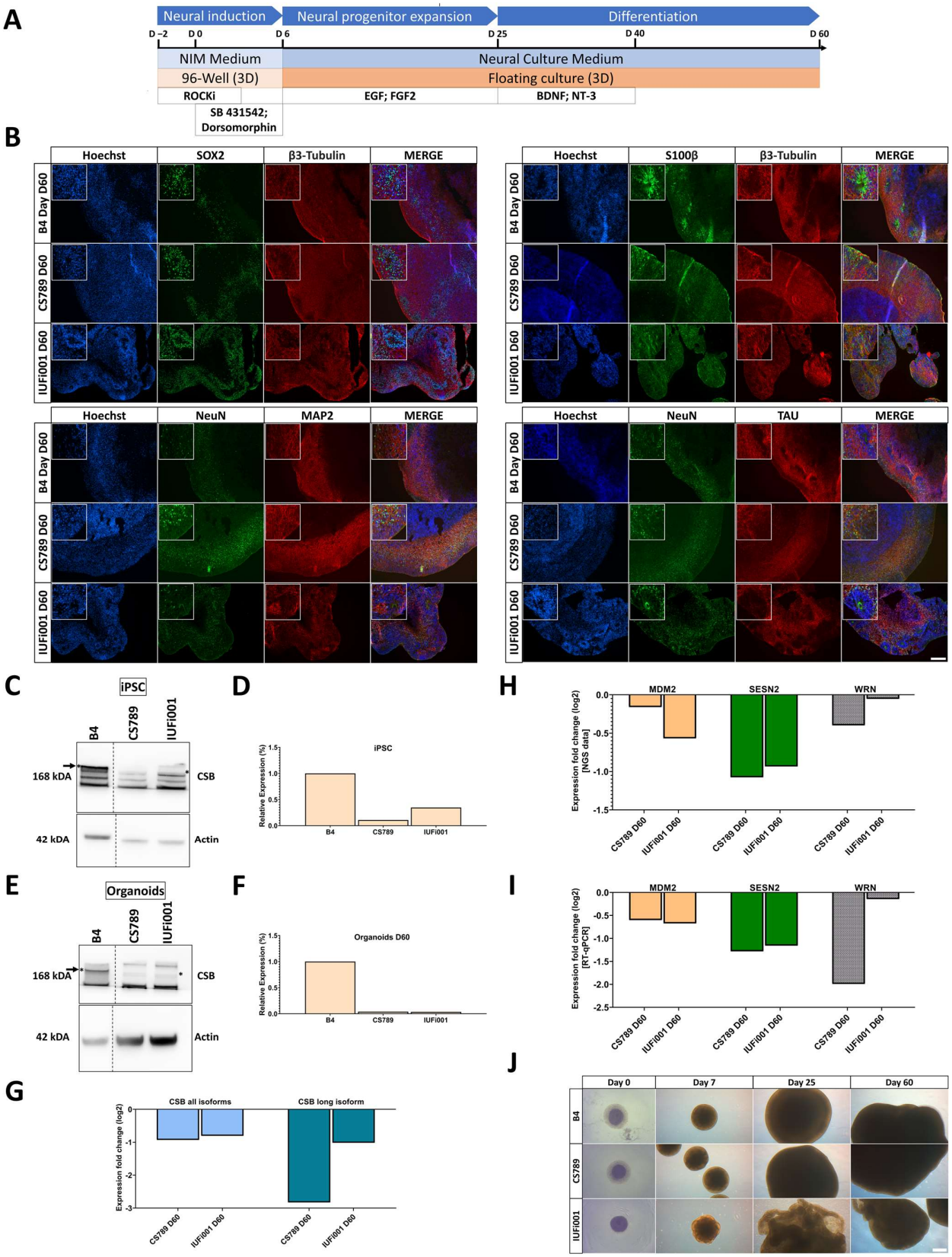

Figure 2. Generation and characterization of CS organoids. (**A**) Schematic outline of the protocol to generate iPSC-derived cerebral organoids. (**B**) Representative immunocytochemistry images of the

distribution of cells expressing SOX2, β3-Tubulin, S100, NeuN, MAP2 and TAU. 100× magnification, scale bar 200 μm. (**C**) Western blot analysis for full-length CSB and beta-actin at the iPSC stage. (**D**) Quantification of CSB Western blot analysis at the iPSC stage in CTRL (B4), CS789 and IUFi001. CSB expression of CS789 and IUFi001 is compared to CSB expression in CTRL (B4) (**E**). Western blot analysis for full-length CSB and beta-actin at day 60 of organoid differentiation. (**F**) Quantification of CSB Western blot analysis at iPSC stage in CTRL (**B**), CS789 and IUFi001. CSB expression of CS789 and IUFi001 is compared to CSB expression in CTRL (B4). (**G**) qRT-PCR analysis of full-length *CSB* mRNA expression and all isoform *CSB* mRNA expression in CS789 and IUFi001 organoids relative to control organoids. (**H**) Relative mRNA expression analysis of DNA damage-related genes *MDM2*, *SESN2* and *WRN* in CS789 and IUFi001 organoids compared to CTRL (B4). (**I**) qRT-PCR analysis of *MDM2*, *SESN2* and *WRN* mRNA expression in CS789 and IUFi001 organoids relative to CTRL (B4). (**J**) Representative brightfield images of control and CS organoids at day 0, 7, 25 and 53 of differentiation. Scale bar 200 μm. (**C**,**E**) Arrows indicate bands of interest. Asterisk (*) indicates height of bands of interest on the right side. Dotted lines indicate excision point of one sample. Full-length blots are presented in Supplementary Figure S3.

These results imply that control and CS patient-derived iPSCs can be efficiently differentiated into NS following our protocol. Patient-derived NS do not seem to exhibit changes in cyto-architecture, cellular makeup or proliferation in comparison to the control.

3.2. Both Control and CSB-iPSCs Efficiently Differentiate into Cerebral Organoids

To elucidate transcriptional regulation at advanced stages of early human neurodevelopment in patients with CS, we also cultured cerebral organoids for 60 days.

By day 60 of differentiation, immunocytochemical staining revealed that both CS and control lines share a common cyto-architecture. The outer layer (~300–500 nm) of these COs is composed of SOX2+ NPCs self-organized into VZ-like structures surrounded by early-born and mature neurons.

The mature neurons are microtubule-associated protein 2 (MAP2)+, microtubule-associated protein tau (TAU)+ and RNA binding fox-1 homolog 3 (NeuN)+ in the COs of all cell lines (Figure 2B). All neurons including the early-born neurons are stained with TUBB3. The staining of S100 calcium-binding protein B (S100B) reveals the presence of radial glial cells and/or early astrocyte progenitors in the COs of all three cell lines.

We performed a Western blot to detect CSB at the iPSC and day 60 CO stage (Figure 2C,E). This revealed markedly reduced levels of CSB in both patient-derived iPSC lines and COs in comparison to the control (Figure 2D,F). The full Western Blot can be found in Supplementary Figure S3. RT-qPCR revealed a ~50% translation reduction of all CSB isoforms in both patient-derived cell lines, a ~90% translation reduction of the full-length isoform in the CS789 line and a ~50% reduction in the IUFi001 line (Figure 2G).

Prior to NGS analysis, we performed RT-qPCR for the genes MDM2 proto-oncogene, E3 ubiquitin protein ligase (*MDM2*), sestrin-2 (*SESN2*) and Werner syndrome RecQ-like helicase (*WRN*), which were expected to be regulated in our patient-derived COs (Figure 2I). The dysregulation was later confirmed by the NGS data (Figure 2H).

Over the course of the CO differentiation, control and CS789 cell lines behaved similarly with respect to growth. The IUFi001 COs flattened and folded early in the differentiation and were broken up into smaller organoids by the shear forces of the spinning incubator (Figure 2J). Still, except for the size, the cyto-architecture of the IUFi001 COs is comparable to the control and CS789 cell line.

By comparing the CO RNA-Seq datasets with datasets from the Allen Brain Atlas, we attempted to determine the developmental age of the COs (Supplementary Figure S2A). We observed that the transcriptomes of the day 60 COs are approximate to 13–21 weeks post-conception foetal brains (Supplementary Figure S2C).

Collectively, these results suggest that control and CS patient-derived iPSCs can efficiently differentiate into COs following our protocol. Patient-derived CS COs do not seem to exhibit major changes in cyto-architecture in comparison to the control and recapitulate

aspects of early human neurodevelopment but present an expected dysregulation of damage-related gene expression.

3.3. CSB Neurospheres of Patients with Different Severity Show Distinct but Partially Overlapping Transcriptome Dysregulation

To gain insight into the early neurodevelopmental transcriptional differences between patients with CS and healthy individuals, we performed transcriptome analysis of the day 30 NS via RNA-Seq. Hierarchical clustering (Supplementary Figure S4A) and principal component analysis (Supplementary Figure S4B) of all datasets (iPSCs, neurospheres and organoids of B4, CS789 and IUFi001) revealed correct clustering of the respective timepoints to each other with no outliers.

Next, we compared the transcriptome of CS789 NS to control NS. We found that 641 genes are exclusively expressed in CS789 NS, 635 genes exclusively expressed in control NS and 14,001 genes expressed in both. Of these commonly expressed 14,001 genes, 2302 genes are upregulated and 430 genes downregulated in CS789 NS in comparison to the control (Figure 3A). With these identified differentially expressed genes (DEGs), we performed an enrichment analysis to identify the most dysregulated Kyoto Encyclopaedia of Genes and Genomes (KEGG) pathways in CS789 NS. The three most upregulated KEGG pathways are the following—*protein processing in endoplasmatic reticulum*, *adherens junction* and *Hippo signalling pathway* (Figure 3C). The three most downregulated KEGG pathways are *ribosome*, *oxidative phosphorylation* and *thermogenesis* (Figure 3D).

Subsequently, the transcriptome of the IUFi001 NS was compared to control NS. We identified 720 genes to be exclusively expressed in IUFi001 NS, 746 genes exclusively expressed in control NS and 13,890 genes expressed in both. Of the commonly expressed 13,890 genes, 1540 genes are upregulated and 723 genes downregulated in IUFi001 NS in comparison to the control (Figure 3B). The three most upregulated KEGG pathways in IUFi001 NS are the following—*protein processing in endoplasmatic reticulum*, *steroid biosynthesis* and *carbon metabolism* (Figure 3E). The three most downregulated KEGG pathways are *ribosome*, *oxidative phosphorylation* and *thermogenesis* (Figure 3F). Since we want to identify dysregulation common to all types of CS, we compared the 50 highest up- and downregulated KEGG pathways in both patient-derived NS in comparison to the control. The five most upregulated KEGG pathways common in CS789 and IUFi001 neurospheres are *protein processing in endoplasmatic reticulum*, *adherens junction*, *Hippo signalling pathway*, *RNA transport* and *Wnt signalling pathway* (Figure 3G).

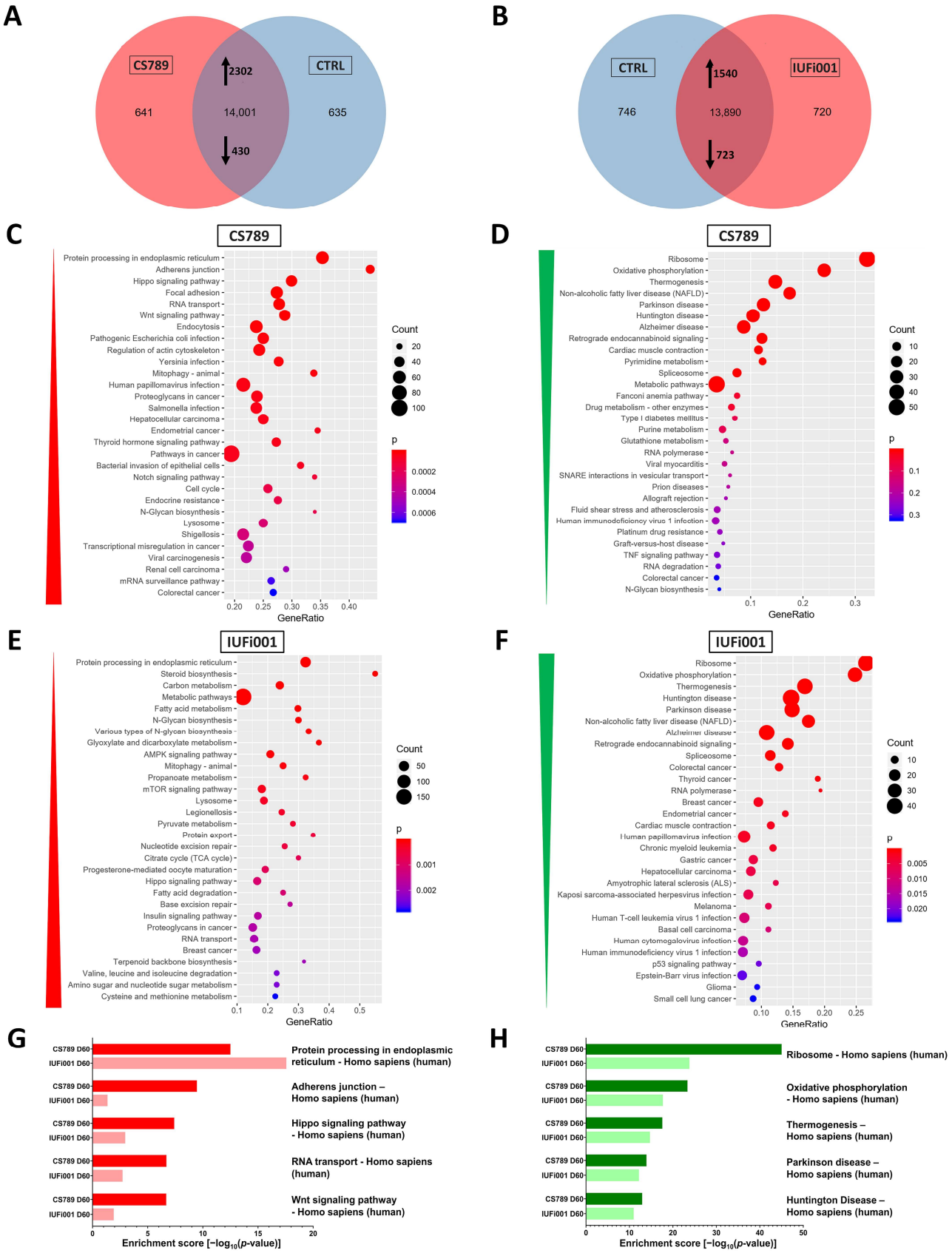
A
CS789
CTRL
641
14,001
635
2302
430
B
CTRL
IUFi001
746
13,890
720
1540
723
C
CS789
Protein processing in endoplasmic reticulum
Adherens junction
Hippo signaling pathway
Focal adhesion
RNA transport
Wnt signaling pathway
Endocytosis
Pathogenic Escherichia coli infection
Regulation of actin cytoskeleton
Yersinia infection
Mitophagy - animal
Human papillomavirus infection
Proteoglycans in cancer
Salmonella infection
Hepatocellular carcinoma
Endometrial cancer
Thyroid hormone signaling pathway
Pathways in cancer
Bacterial invasion of epithelial cells
Notch signaling pathway
Cell cycle
Endocrine resistance
N-Glycan biosynthesis
Lysosome
Shigellosis
Transcriptional misregulation in cancer
Viral carcinogenesis
Renal cell carcinoma
mRNA surveillance pathway
Colorectal cancer
0.20 0.25 0.30 0.35 0.40
GeneRatio
Count
20
40
60
80
100
p
0.0002
0.0004
0.0006
D
CS789
Ribosome
Oxidative phosphorylation
Thermogenesis
Non-alcoholic fatty liver disease (NAFLD)
Parkinson disease
Huntington disease
Alzheimer disease
Retrograde endocannabinoid signaling
Cardiac muscle contraction
Pyrimidine metabolism
Spliceosome
Metabolic pathways
Fanconi anemia pathway
Drug metabolism - other enzymes
Type I diabetes mellitus
Purine metabolism
Glutathione metabolism
RNA polymerase
Viral myocarditis
SNARE interactions in vesicular transport
Prion diseases
Allograft rejection
Fluid shear stress and atherosclerosis
Human immunodeficiency virus 1 infection
Platinum drug resistance
Graft-versus-host disease
TNF signaling pathway
RNA degradation
Colorectal cancer
N-Glycan biosynthesis
0.1 0.2 0.3
GeneRatio
Count
10
20
30
40
50
p
0.1
0.2
0.3
E
IUFi001
Protein processing in endoplasmic reticulum
Steroid biosynthesis
Carbon metabolism
Metabolic pathways
Fatty acid metabolism
N-Glycan biosynthesis
Various types of N-glycan biosynthesis
Glyoxylate and dicarboxylate metabolism
AMPK signaling pathway
Mitophagy - animal
Propanoate metabolism
mTOR signaling pathway
Lysosome
Legionellosis
Pyruvate metabolism
Protein export
Nucleotide excision repair
Citrate cycle (TCA cycle)
Progesterone-mediated oocyte maturation
Hippo signaling pathway
Fatty acid degradation
Base excision repair
Insulin signaling pathway
Proteoglycans in cancer
RNA transport
Breast cancer
Terpenoid backbone biosynthesis
Valine, leucine and isoleucine degradation
Amino sugar and nucleotide sugar metabolism
Cysteine and methionine metabolism
0.1 0.2 0.3 0.4 0.5
GeneRatio
Count
50
100
150
p
0.001
0.002
F
IUFi001
Ribosome
Oxidative phosphorylation
Thermogenesis
Huntington disease
Parkinson disease
Non-alcoholic fatty liver disease (NAFLD)
Alzheimer disease
Retrograde endocannabinoid signaling
Spliceosome
Colorectal cancer
Thyroid cancer
RNA polymerase
Breast cancer
Endometrial cancer
Cardiac muscle contraction
Human papillomavirus infection
Chronic myeloid leukemia
Gastric cancer
Hepatocellular carcinoma
Amyotrophic lateral sclerosis (ALS)
Kaposi sarcoma-associated herpesvirus infection
Melanoma
Human T-cell leukemia virus 1 infection
Basal cell carcinoma
Human cytomegalovirus infection
Human immunodeficiency virus 1 infection
p53 signaling pathway
Epstein-Barr virus infection
Glioma
Small cell lung cancer
0.10 0.15 0.20 0.25
GeneRatio
Count
10
20
30
40
p
0.005
0.010
0.015
0.020
G
CS789 D60
IUFi001 D60
Protein processing in endoplasmic reticulum - Homo sapiens (human)
Adherens junction – Homo sapiens (human)
Hippo signaling pathway - Homo sapiens (human)
RNA transport - Homo sapiens (human)
Wnt signaling pathway - Homo sapiens (human)
0 5 10 15 20
Enrichment score [−log10(p-value)]
H
CS789 D60
IUFi001 D60
Ribosome - Homo sapiens (human)
Oxidative phosphorylation - Homo sapiens (human)
Thermogenesis – Homo sapiens (human)
Parkinson disease – Homo sapiens (human)
Huntington Disease – Homo sapiens (human)
0 10 20 30 40 50
Enrichment score [−log10(p-value)]

Figure 3. Global transcriptome and associated pathway analysis of control and CS neurospheres at day 30. (**A**) Venn diagram showing genes expressed only in CS789 neurospheres (641), in CTRL (B4) neurospheres (635) and common to both (14,001) (detection p value < 0.05). (**B**) Venn diagram showing genes expressed only in IUFi001 neurospheres (720), in CTRL (B4) neurospheres (746) and common to both (13,890) (detection p value < 0.05). (**C**,**D**) Dot plots showing the top 30 differentially regulated KEGG pathways (**C**) in the 2302 significantly upregulated DEGs in day 30 CS789 neurospheres in comparison to CTRL (B4) (**D**) and in the 430 significantly downregulated DEGs in day 30 CS789 neurospheres in comparison to CTRL (B4). (**E**,**F**) Dot plots showing the top 30 differentially regulated KEGG pathways (**E**) in the 1540 significantly upregulated DEGs in day 30 IUFi001 neurospheres in comparison to CTRL (B4) (**F**) and in the 723 significantly downregulated DEGs in day 30 IUFi001 neurospheres in comparison to CTRL (B4). (**G**) Bar chart of the differentially upregulated KEGG pathways (top five ranked) common between day 30 CS789 and IUFi001 neurospheres in comparison to CTRL (B4) neurospheres. (**H**) Bar chart of the differentially downregulated KEGG pathways (top five ranked) common between day 30 CS789 and IUFi001 neurospheres in comparison to CTRL (B4) neurospheres.

The five most downregulated KEGG pathways common in CS789 and IUFi001 neurospheres are *ribosome*, *oxidative phosphorylation*, *thermogenesis*, *Parkinson's disease* and *Huntington's disease* (Figure 3H). The complete list of pathways common in the 50 most severely dysregulated KEGG pathways can be found in Supplemental Table S2.

These results indicate that while there are ample differences in gene expression between distinct individuals and severity grades of CS, there is also common dysregulation. And, while most symptoms manifest only postnatally in all but the most severe form of CS, this common dysregulation can already be detected in carriers of less severe forms at the NPC stage.

3.4. CSB Organoids of Patients with Different Severity Show Distinct but Partially Overlapping Transcriptome Dysregulation

To investigate the molecular differences between patients with CS and healthy individuals at a more advanced stage of brain development (BD), we performed transcriptome analysis of the day 60 cerebral organoids.

We first compared the transcriptome of the CS789 COs to control COs. We identified 443 genes as exclusively expressed in CS789 COs, 1006 genes exclusively expressed in control COs and 14,030 genes expressed in both. Of these commonly expressed 14,030 genes, 373 genes are upregulated and 2163 downregulated in CS789 COs in comparison to the control (Figure 4A). We utilized the DEGs to perform an enrichment analysis to identify the most dysregulated KEGG pathways in CS789 COs. The three most upregulated KEGG pathways are *ribosome*, *steroid biosynthesis* and *terpenoid backbone biosynthesis* (Figure 4C). The three most downregulated KEGG pathways are *axon guidance*, the *Wnt signalling pathway* and *synaptic vesicle cycle* (Figure 4D).

Next, the transcriptome of the IUFi001 COs was compared to control COs. We identified 674 genes as exclusively expressed in IUFi001 COs, 610 genes exclusively expressed in control COs and 14,426 genes expressed in both. Of these 14,426 commonly expressed genes, 930 genes are upregulated, and 1687 downregulated in IUFi001 organoids in comparison to the control (Figure 4B). The three most upregulated KEGG pathways are *protein processing in endoplasmatic reticulum*, *metabolic pathways* and *pathways in cancer* (Figure 4E). The three most downregulated KEGG pathways are *axon guidance*, *the synaptic vesicle cycle* and *glutamatergic synapse* (Figure 4F).

We again compared the 50 highest up- and downregulated KEGG pathways in both patient-derived COs in comparison to the control. The five most upregulated KEGG pathways common in CS789 and IUFi001 COs are *steroid biosynthesis*, *p53 signalling pathway*, *breast cancer*, *terpenoid backbone biosynthesis* and *antigen processing and presentation.* (Figure 4G). The five most downregulated KEGG pathways common in CS789 and IUFi001 COs are *axon guidance*, *synaptic vesicle cycle*, *glutamatergic synapse*, *Wnt signalling pathway* and *signalling pathways regulating pluripotency of stem cells* (Figure 4H).

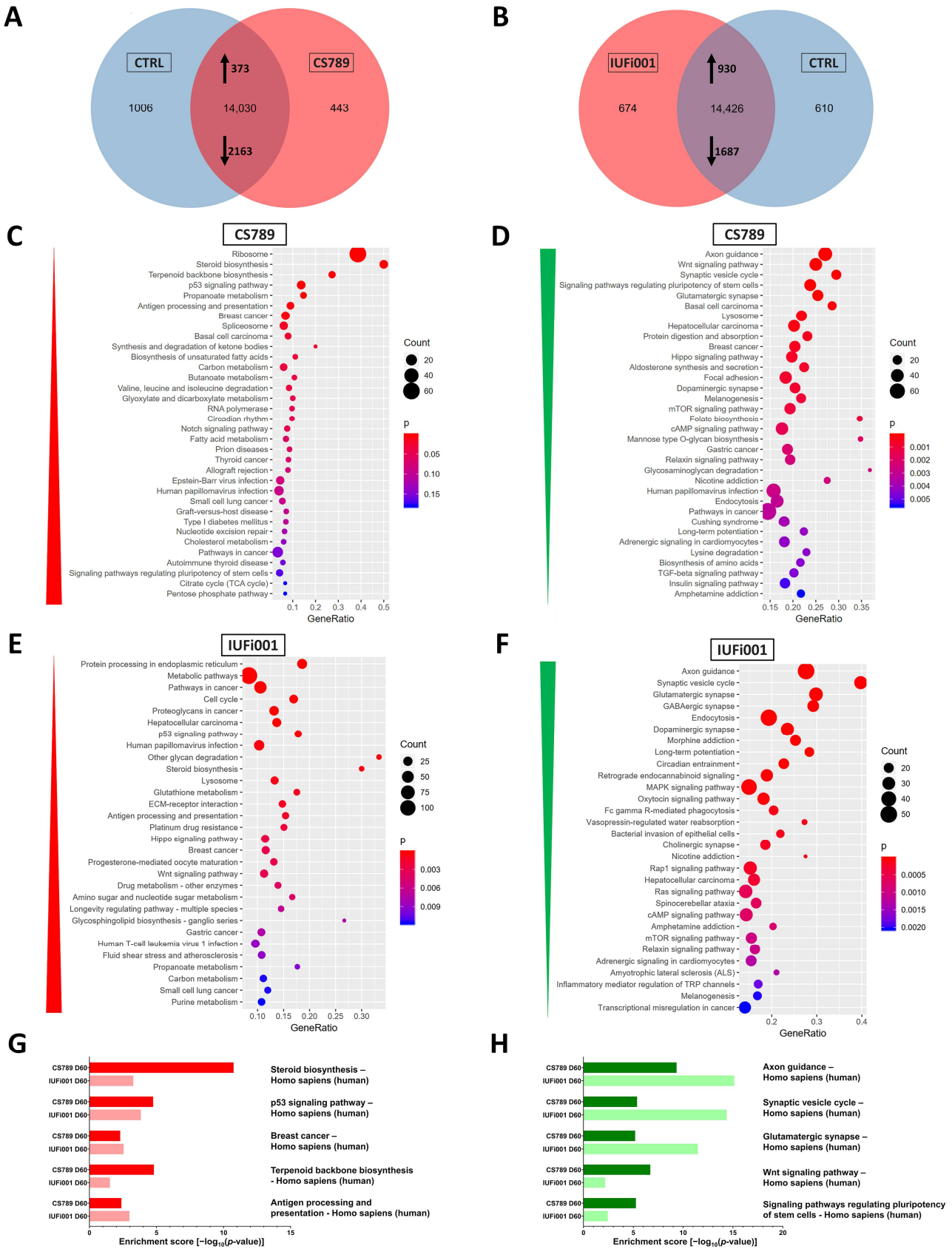
A
CTRL
CS789
1006
373
14,030
2163
443
B
IUFi001
CTRL
674
930
14,426
1687
610
C
CS789
Ribosome
Steroid biosynthesis
Terpenoid backbone biosynthesis
p53 signaling pathway
Propanoate metabolism
Antigen processing and presentation
Breast cancer
Spliceosome
Basal cell carcinoma
Synthesis and degradation of ketone bodies
Biosynthesis of unsaturated fatty acids
Carbon metabolism
Butanoate metabolism
Valine, leucine and isoleucine degradation
Glyoxylate and dicarboxylate metabolism
RNA polymerase
Circadian rhythm
Notch signaling pathway
Fatty acid metabolism
Prion diseases
Thyroid cancer
Allograft rejection
Epstein-Barr virus infection
Human papillomavirus infection
Small cell lung cancer
Graft-versus-host disease
Type I diabetes mellitus
Nucleotide excision repair
Cholesterol metabolism
Pathways in cancer
Autoimmune thyroid disease
Signaling pathways regulating pluripotency of stem cells
Citrate cycle (TCA cycle)
Pentose phosphate pathway
0.1 0.2 0.3 0.4 0.5
GeneRatio
Count
20
40
60
p
0.05
0.10
0.15
D
CS789
Axon guidance
Wnt signaling pathway
Synaptic vesicle cycle
Signaling pathways regulating pluripotency of stem cells
Glutamatergic synapse
Basal cell carcinoma
Lysosome
Hepatocellular carcinoma
Protein digestion and absorption
Breast cancer
Hippo signaling pathway
Aldosterone synthesis and secretion
Focal adhesion
Dopaminergic synapse
Melanogenesis
mTOR signaling pathway
Folate biosynthesis
cAMP signaling pathway
Mannose type O-glycan biosynthesis
Gastric cancer
Relaxin signaling pathway
Glycosaminoglycan degradation
Nicotine addiction
Human papillomavirus infection
Endocytosis
Pathways in cancer
Cushing syndrome
Long-term potentiation
Adrenergic signaling in cardiomyocytes
Lysine degradation
Biosynthesis of amino acids
TGF-beta signaling pathway
Insulin signaling pathway
Amphetamine addiction
0.15 0.20 0.25 0.30 0.35
GeneRatio
Count
20
40
60
p
0.001
0.002
0.003
0.004
0.005
E
IUFi001
Protein processing in endoplasmic reticulum
Metabolic pathways
Pathways in cancer
Cell cycle
Proteoglycans in cancer
Hepatocellular carcinoma
p53 signaling pathway
Human papillomavirus infection
Other glycan degradation
Steroid biosynthesis
Lysosome
Glutathione metabolism
ECM-receptor interaction
Antigen processing and presentation
Platinum drug resistance
Hippo signaling pathway
Breast cancer
Progesterone-mediated oocyte maturation
Wnt signaling pathway
Drug metabolism - other enzymes
Amino sugar and nucleotide sugar metabolism
Longevity regulating pathway - multiple species
Glycosphingolipid biosynthesis - ganglio series
Gastric cancer
Human T-cell leukemia virus 1 infection
Fluid shear stress and atherosclerosis
Propanoate metabolism
Carbon metabolism
Small cell lung cancer
Purine metabolism
0.10 0.15 0.20 0.25 0.30
GeneRatio
Count
25
50
75
100
p
0.003
0.006
0.009
F
IUFi001
Axon guidance
Synaptic vesicle cycle
Glutamatergic synapse
GABAergic synapse
Endocytosis
Dopaminergic synapse
Morphine addiction
Long-term potentiation
Circadian entrainment
Retrograde endocannabinoid signaling
MAPK signaling pathway
Oxytocin signaling pathway
Fc gamma R-mediated phagocytosis
Vasopressin-regulated water reabsorption
Bacterial invasion of epithelial cells
Cholinergic synapse
Nicotine addiction
Rap1 signaling pathway
Hepatocellular carcinoma
Ras signaling pathway
Spinocerebellar ataxia
cAMP signaling pathway
Amphetamine addiction
mTOR signaling pathway
Relaxin signaling pathway
Adrenergic signaling in cardiomyocytes
Amyotrophic lateral sclerosis (ALS)
Inflammatory mediator regulation of TRP channels
Melanogenesis
Transcriptional misregulation in cancer
0.2 0.3 0.4
GeneRatio
Count
20
30
40
50
p
0.0005
0.0010
0.0015
0.0020
G
CS789 D60
IUFi001 D60
Steroid biosynthesis – Homo sapiens (human)
p53 signaling pathway – Homo sapiens (human)
Breast cancer – Homo sapiens (human)
Terpenoid backbone biosynthesis - Homo sapiens (human)
Antigen processing and presentation - Homo sapiens (human)
0 5 10 15
Enrichment score [−log10(p-value)]
H
CS789 D60
IUFi001 D60
Axon guidance – Homo sapiens (human)
Synaptic vesicle cycle – Homo sapiens (human)
Glutamatergic synapse – Homo sapiens (human)
Wnt signaling pathway – Homo sapiens (human)
Signaling pathways regulating pluripotency of stem cells - Homo sapiens (human)
0 5 10 15 20
Enrichment score [−log10(p-value)]

Figure 4. Global transcriptome and associated pathway analysis of control and CS organoids at day 60. (**A**) Venn diagram showing genes expressed only in CS789 organoids (443), in CTRL (B4) organoids (1006) and common to both (14,030) (detection p value < 0.05). (**B**) Venn diagram showing genes expressed only in IUFi001 organoids (674), in CTRL (B4) organoids (610) and common to both (14,426) (detection p value < 0.05). (**C**,**D**) Dot plots showing the top 30 differentially regulated KEGG pathways (**C**) in the 373 significantly upregulated DEGs in day 60 CS789 organoids in comparison to CTRL (B4) (**D**) and in the 2163 significantly downregulated DEGs in day 60 CS789 organoids in comparison to CTRL (B4). (**E**,**F**) Dot plots showing the top 30 differentially regulated KEGG pathways (**E**) in the 930 significantly upregulated DEGs in day 60 IUFi001 organoids in comparison to CTRL (B4) (**F**) and in the 1687 significantly downregulated DEGs in day 60 IUFi001 organoids in comparison to CTRL (B4). (**G**) Bar chart of the differentially upregulated KEGG pathways (top five ranked) common between day 60 CS789 and IUFi001 organoids in comparison to CTRL (B4) organoids. (**H**) Bar chart of the differentially downregulated KEGG pathways (top five ranked) common between day 60 CS789 and IUFi001 organoids in comparison to CTRL (B4) organoids.

The complete list of pathways common in the 50 most severely dysregulated KEGG pathways can be found in Supplemental Table S2.

These results imply that while there are ample differences in gene expression between distinct individuals and severity grades of CS at the later stages of BD, there is also severe common dysregulation, especially the downregulation of genes important for BD and neuronal function. As with the neurospheres, this common dysregulation can already be detected in carriers of less severe forms of CS in the early stages of BD.

3.5. Non-Redundant Enrichment Analysis Reveals Dysregulation of VEGFA-VEGFR2 Signalling, Brain Development and Intracellular Transport in CSB Neurospheres

We performed an analysis of the dysregulated gene ontologies (GOs) in our CS NS in comparison to the control (Supplementary Figure S5). A variety of often related GOs were unveiled. To generate a clearer picture of the dysregulation in our CS neurospheres, the more extensive, upregulated gene sets (CS789 2302 genes; IUFi001 1540 genes) were subjected to Metascape-based analysis, which resulted in non-redundant enrichment clusters. An analysis of the downregulated gene sets can be found in Supplementary Figure S6.

For the CS789 NS, the three most enriched clusters were the *VEGFA-VEGFR2 signalling pathway*, *cell morphogenesis* and *head development* (Figure 5A). For the IUFi001 NS, the three most enriched clusters were *vesicle-mediated transport*, *intracellular protein transport* and *protein processing in endoplasmatic reticulum* (Figure 5B).

To pinpoint pathways of interest, we compared both gene sets employing Metascape-based analysis. The highest consensus can be observed in *vesicle-mediated transport*, *cell cycle*, the *VEGFA-VEGFR2 signalling pathway*, *intracellular protein transport* and *cellular responses to stress* (Figure 5C). A manual comparison of the singular analyses in Figure 5A,B revealed identical enrichment clusters to the Metascape-based comparison (Figure 5D).

Next, we chose the Reactome set *vesicle-mediated transport* and the GOs *intracellular protein transport* and *head development*, compared the corresponding gene lists of both patient-derived NS and extracted the genes similarly regulated in comparison to the control. This resulted in 165 genes for *intracellular protein transport*, 139 genes for *vesicle-mediated transport* and 82 genes for *head development*. The resulting gene sets were compared utilizing Pearson's heatmap analysis (Supplementary Figure S7). These gene sets were then reduced to the 40 highest dysregulated genes common between both patient-derived NS (Figure 5E–G).

These results imply that at the developmental stage of NPCs, there is severe dysregulation pertaining to distinct intracellular transport mechanisms, the coordination of cell cycles and protein metabolism common between distinct grades of severity in patients with CS.

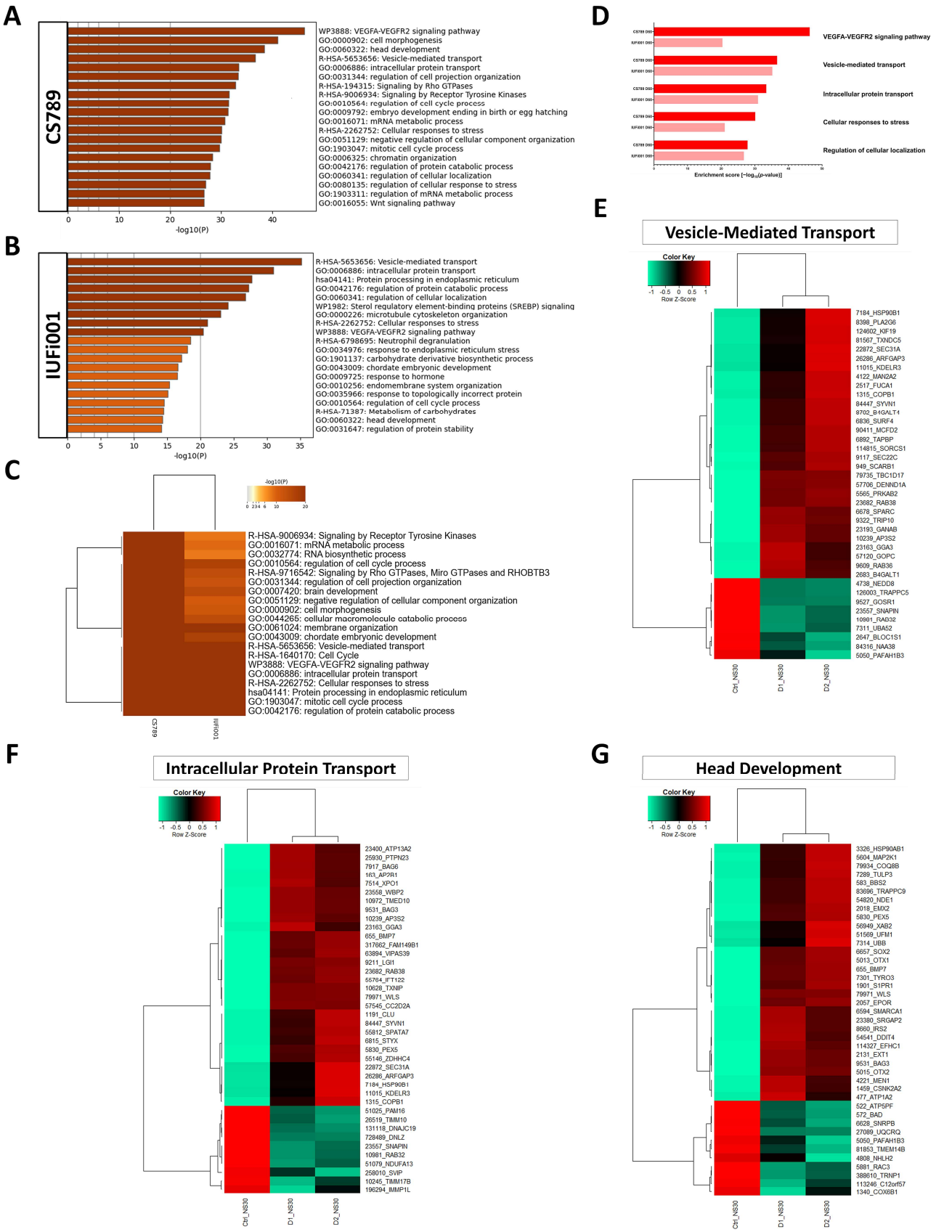
A
CS789
WP3888: VEGFA-VEGFR2 signaling pathway
GO:0000902: cell morphogenesis
GO:0060322: head development
R-HSA-5653656: Vesicle-mediated transport
GO:0006886: intracellular protein transport
GO:0031344: regulation of cell projection organization
R-HSA-194315: Signaling by Rho GTPases
R-HSA-9006934: Signaling by Receptor Tyrosine Kinases
GO:0010564: regulation of cell cycle process
GO:0009792: embryo development ending in birth or egg hatching
GO:0016071: mRNA metabolic process
R-HSA-2262752: Cellular responses to stress
GO:0051129: negative regulation of cellular component organization
GO:1903047: mitotic cell cycle process
GO:0006325: chromatin organization
GO:0042176: regulation of protein catabolic process
GO:0060341: regulation of cellular localization
GO:0080135: regulation of cellular response to stress
GO:1903311: regulation of mRNA metabolic process
GO:0016055: Wnt signaling pathway
0 10 20 30 40
-log10(P)
B
IUFi001
R-HSA-5653656: Vesicle-mediated transport
GO:0006886: intracellular protein transport
hsa04141: Protein processing in endoplasmic reticulum
GO:0042176: regulation of protein catabolic process
GO:0060341: regulation of cellular localization
WP1982: Sterol regulatory element-binding proteins (SREBP) signaling
GO:0000226: microtubule cytoskeleton organization
R-HSA-2262752: Cellular responses to stress
WP3888: VEGFA-VEGFR2 signaling pathway
R-HSA-6798695: Neutrophil degranulation
GO:0034976: response to endoplasmic reticulum stress
GO:1901137: carbohydrate derivative biosynthetic process
GO:0043009: chordate embryonic development
GO:0009725: response to hormone
GO:0010256: endomembrane system organization
GO:0035966: response to topologically incorrect protein
GO:0010564: regulation of cell cycle process
R-HSA-71387: Metabolism of carbohydrates
GO:0060322: head development
GO:0031647: regulation of protein stability
0 5 10 15 20 25 30 35
-log10(P)
C
-log10(P)
0 2 3 4 6 10 20
R-HSA-9006934: Signaling by Receptor Tyrosine Kinases
GO:0016071: mRNA metabolic process
GO:0032774: RNA biosynthetic process
GO:0010564: regulation of cell cycle process
R-HSA-9716542: Signaling by Rho GTPases, Miro GTPases and RHOBTB3
GO:0031344: regulation of cell projection organization
GO:0007420: brain development
GO:0051129: negative regulation of cellular component organization
GO:0000902: cell morphogenesis
GO:0044265: cellular macromolecule catabolic process
GO:0061024: membrane organization
GO:0043009: chordate embryonic development
R-HSA-5653656: Vesicle-mediated transport
R-HSA-1640170: Cell Cycle
WP3888: VEGFA-VEGFR2 signaling pathway
GO:0006886: intracellular protein transport
R-HSA-2262752: Cellular responses to stress
hsa04141: Protein processing in endoplasmic reticulum
GO:1903047: mitotic cell cycle process
GO:0042176: regulation of protein catabolic process
CS789
IUFi001
D
CS789 DMSO
IUFi001 DMSO
VEGFA-VEGFR2 signaling pathway
Vesicle-mediated transport
Intracellular protein transport
Cellular responses to stress
Regulation of cellular localization
Enrichment score [−log10(p-value)]
E
Vesicle-Mediated Transport
Color Key
-1 -0.5 0 0.5 1
Row Z-Score
7184_HSP90B1
8398_PLA2G6
124602_KIF19
81567_TXNDC5
22872_SEC31A
26286_ARFGAP3
11015_KDELR3
4122_MAN2A2
2517_FUCA1
1315_COPB1
84447_SYVN1
8702_B4GALT4
6836_SURF4
90411_MCFD2
6892_TAPBP
114815_SORCS1
9117_SEC22C
949_SCARB1
79735_TBC1D17
57706_DENND1A
5565_PRKAB2
23682_RAB38
6678_SPARC
9322_TRIP10
23193_GANAB
10239_AP3S2
23163_GGA3
57120_GOPC
9609_RAB36
2683_B4GALT1
4738_NEDD8
126003_TRAPPC5
9527_GOSR1
23557_SNAPIN
10981_RAB32
7311_UBA52
2647_BLOC1S1
84316_NAA38
5050_PAFAH1B3
Ctrl_NS30
D1_NS30
D2_NS30
F
Intracellular Protein Transport
Color Key
-1 -0.5 0 0.5 1
Row Z-Score
23400_ATP13A2
25930_PTPN23
7917_BAG6
163_AP2B1
7514_XPO1
23558_WBP2
10972_TMED10
9531_BAG3
10239_AP3S2
23163_GGA3
655_BMP7
317662_FAM149B1
63894_VIPAS39
9211_LGI1
23682_RAB38
55764_IFT122
10628_TXNIP
79971_WLS
57545_CC2D2A
1191_CLU
84447_SYVN1
51812_SPATA7
6815_STYX
5830_PEX5
55146_ZDHHC4
22872_SEC31A
26286_ARFGAP3
7184_HSP90B1
11015_KDELR3
1315_COPB1
51025_PAM16
26519_TIMM10
131118_DNAJC19
728489_DNLZ
23557_SNAPIN
10981_RAB32
51079_NDUFA13
258010_SVIP
10245_TIMM17B
196294_IMMP1L
Ctrl_NS30
D1_NS30
D2_NS30
G
Head Development
Color Key
-1 -0.5 0 0.5 1
Row Z-Score
3326_HSP90AB1
5604_MAP2K1
79934_COQ8B
7289_TULP3
583_BBS2
83696_TRAPPC9
54820_NDE1
2018_EMX2
5830_PEX5
56949_XAB2
51569_UFM1
7314_UBB
6657_SOX2
5013_OTX1
655_BMP7
7301_TYRO3
1901_S1PR1
79971_WLS
2057_EPOR
6594_SMARCA1
23380_SRGAP2
8660_IRS2
54541_DDIT4
114327_EFHC1
2131_EXT1
9531_BAG3
5015_OTX2
4221_MEN1
1459_CSNK2A2
477_ATP1A2
522_ATP5PF
572_BAD
6628_SNRPB
27089_UQCRQ
5050_PAFAH1B3
81853_TMEM14B
4808_NHLH2
5881_RAC3
388610_TRNP1
113246_C12orf57
1340_COX6B1
Ctrl_NS30
D1_NS30
D2_NS30

Figure 5. Comparative transcriptome and gene ontology analysis of upregulated DEGs in day 30 neurospheres. (**A**) Bar graph of the top 20 non-redundant enrichment clusters attributable to the 2302 DEGs upregulated in day 30 CS789 neurospheres in comparison to CTRL (B4). (**B**) Bar graph of the top 20 non-redundant enrichment clusters attributable to the 1540 DEGs upregulated in day 30 IUFi001 neurospheres. (**C**) Metascape-generated heatmap comparing upregulated gene sets employed in A and B revealed i.a. GOs involved in brain development, intracellular transport and cell cycle. (**D**) Bar chart of the differentially upregulated enrichment clusters (top five ranked) common between day 30 CS789 and IUFi001 neurospheres in comparison to CTRL (B4) neurospheres. (**E**) Pearson's heatmap depicting the 40 most dysregulated genes involved in vesicle-mediated transport common between day 30 CS789 and IUFi001 neurospheres in comparison to CTRL (B4). (**F**) Pearson's heatmap depicting the 40 most dysregulated genes involved in intracellular protein transport common between day 30 CS789 and IUFi001 neurospheres in comparison to CTRL (B4). (**G**) Pearson's heatmap depicting the 40 most dysregulated genes involved in head development common between day 30 CS789 and IUFi001 neurospheres in comparison to CTRL (B4).

3.6. Non-Redundant Enrichment Analysis Reveals Dysregulation of Neuron Projection Development, Brain Development and Distinct Synaptic Pathways in CSB Organoids

Furthermore, we performed an analysis of the dysregulated GOs in our CS COs in comparison to the control (Supplementary Figure S8). Again, a variety of often related GOs were unveiled. To produce a clearer picture of the dysregulation, the more extensive, downregulated gene sets (CS789 2163 genes; IUFi001 1687 genes) were subjected to Metascape-based analysis, which results in non-redundant enrichment clusters. An analysis of the upregulated gene sets can be found in Figure S9.

For the CS789 COs, the three highest rated enrichment clusters were *neuron projection development*, *brain development* and *regulation of neuron projection development* (Figure 6A). For the IUFi001 COs, the three highest rated enrichment clusters were neuron *projection development*, *regulation of trans-synaptic signalling* and *brain development* (Figure 6B). To pinpoint pathways of interest, we compared both gene sets employing Metascape-based analysis. The highest consensus can be observed in *brain development*, *neuronal system*, *cell junction organization*, *regulation of trans-synaptic signalling* and *regulation of synapse structure or activity* (Figure 6C). A manual comparison of the singular analyses in Figure 6A and B revealed identical enrichment clusters to the Metascape-based comparison (Figure 6D).

Subsequently, we chose the GOs *neuron projection development*, *synaptic signalling* and *brain development*, compared the corresponding gene sets of both patient-derived COs and extracted the genes dysregulated in both patient-derived cell lines in comparison to the control. This resulted in 165 genes for *neuron projection development*, 131 genes for *synaptic signalling* and 117 genes for *brain development*. The resulting gene sets were compared utilizing Pearson's heatmap analysis (Supplementary Figure S10). These gene sets were then reduced to the 40 highest regulated genes common between both patient-derived COs (Figure 6E–G).

These results indicate that at the developmental stage of early BD, there is severe dysregulation pertaining to neuron projection development, synaptic function and maintenance and even overall BD.

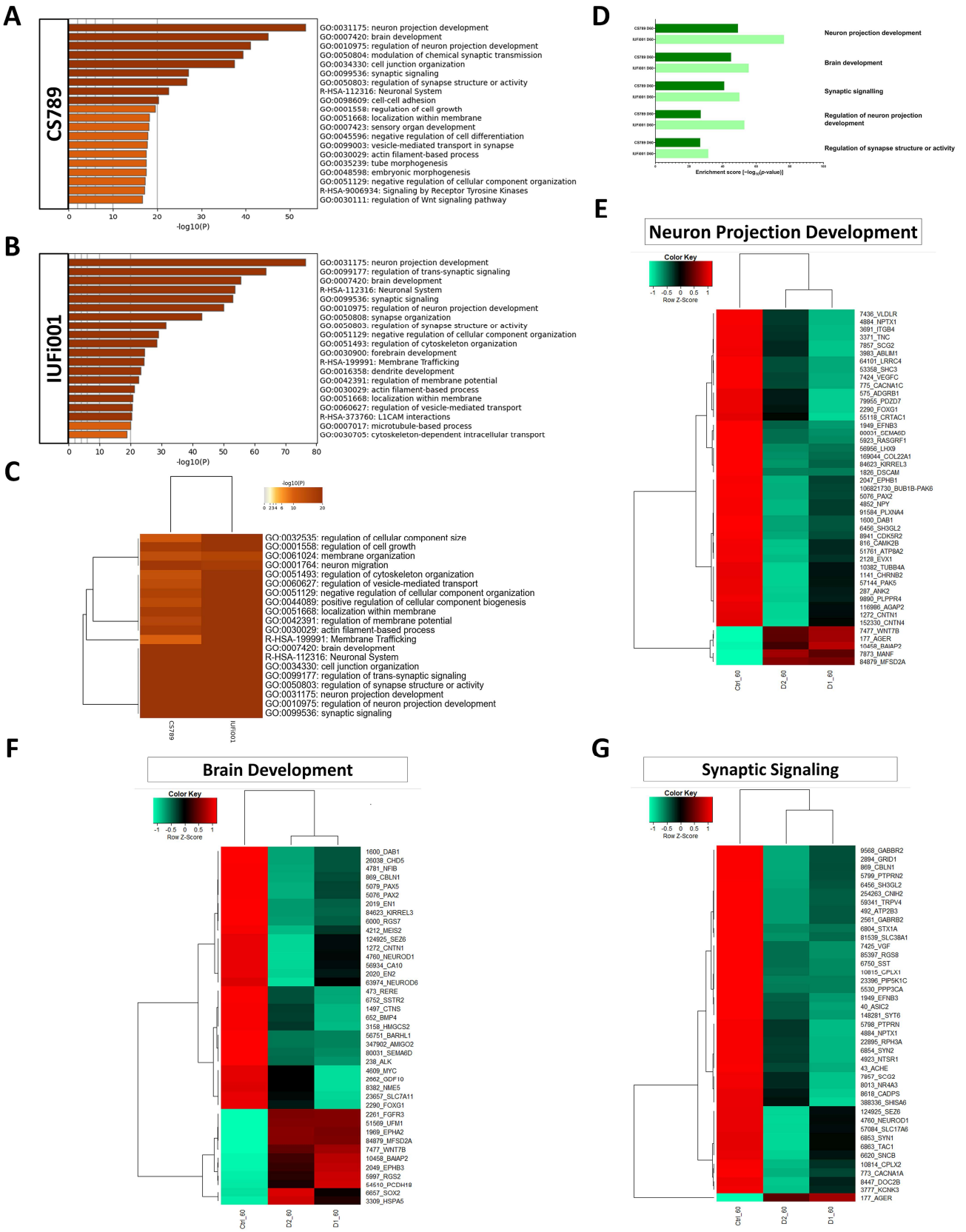

Figure 6. Comparative transcriptome and gene ontology analysis of downregulated DEGs in day 60 organoids. (**A**) Bar graph of the top 20 non-redundant enrichment clusters attributable to the 2163

DEGs downregulated in day 60 CS789 (D1) organoids in comparison to CTRL (B4). (**B**) Bar graph of the top 20 non-redundant enrichment clusters attributable to the 1687 DEGs downregulated in day 60 IUFi001 organoids. (**C**) Metascape-generated heatmap comparing downregulated gene sets employed in A and B revealed i.a. GOs involved in brain development, cell junction organization, neuron projection development and synaptic signalling. (**D**) Bar chart of the differentially downregulated enrichment clusters (top five ranked) common between day 30 CS789 and IUFi001 neurospheres in comparison to CTRL (B4) neurospheres. (**E**) Pearson's heatmap depicting the 45 most dysregulated genes involved in neuron projection development common between day 60 CS789 and IUFi001 organoids in comparison to CTRL (B4). (**F**) Pearson's heatmap depicting the 40 most dysregulated genes involved in brain development common between day 60 CS789 and IUFi001 organoids in comparison to CTRL (B4). (**G**) Pearson's heatmap depicting the 40 most dysregulated genes involved in synaptic signalling common between day 60 CS789 and IUFi001 organoids in comparison to CTRL (B4).

3.7. Non-Redundant Enrichment Analysis of Genes Commonly Regulated at Both Timepoints Reveals Steroid Biosynthesis as Most Severely Affected

We were interested in the genes and associated pathways commonly dysregulated at both developmental timepoints. We pooled the RNA-Seq data of both patient-derived samples at the NS and CO stage and compared them to their respective control via Fisher´s exact test to determine the significantly regulated genes at both timepoints. Next, we compared the resulting gene sets to find genes commonly dysregulated between both timepoints.

The list of commonly dysregulated genes was then subjected to Metascape-based analysis (Figure 7A).

The highest commonly dysregulated enrichment cluster is the KEGG *pathway steroid biosynthesis* and partially overlapping with it, in sixth and eighth place, the Reactome set *activation of gene expression by SREBF (SREBP)* and the GO *fatty acid metabolism*. Other than that, there are three enrichment clusters we examined before, namely, the GOs *synaptic signalling* and *brain development*, as well as the Reactome set *COPII-mediated vesicle transport*.

Next, we investigated which of the commonly dysregulated genes are most severely regulated in both patient-derived lines at both timepoints in comparison to the control. We found that the genes MAGE family member A4 (*MAGEA4*), transmembrane protein 132C (*TMEM132C*), zinc finger protein 558 (*ZNF558*) and tripartite motif containing 4 (*TRIM4*) are the most severely and consistently regulated genes in all patient-derived samples (Supplementary Figure S11A,C,E,G).

After identifying these four genes, we ascertained our findings via RT-qPCR (Supplementary Figure S11B,D,F,H). We further investigated these four genes in another sets of day 60 COs, produced employing an altered media composition. In these COs, we detected the regulation *of MAGEA4*, *TMEM132C*, *ZNF558* and *TRIM4* akin to our initial dataset (Supplementary Figure S11I-L). We cultivated a small number of COs from the initial batch investigated in this work until day 120. The RT-qPCR of these samples also revealed the regulation of these four genes (Supplementary Figure S11M-P).

Following up on our initial Metascape-based analysis, we identified regulated genes involved in cholesterol biosynthesis (CB) in the KEGG pathway steroid biosynthesis at both timepoints. As CB requires the metabolite farnesyl pyrophosphate, we simultaneously investigated the mevalonate pathway branch of terpenoid backbone synthesis at both timepoints. While we found no significantly regulated genes in the NS, an analysis of the CO datasets revealed the regulation of hydroxymethylglutaryl-CoA synthase (*HMGCS*), hydroxymethylglutaryl-CoA reductase (*HMGCR*), one of the rate-limiting enzymes of CB, as well as isopentenyl-diphosphate delta-isomerase (*IDI*) and farnesyl diphosphate synthase (*FDPS*) (Supplementary Figure S12). An analysis of the CB branch of the KEGG pathway steroid biosynthesis indicated the second rate-limiting enzyme of CB squalene epoxidase (*SQLE*) and methylsterol mono-oxygenase (*MSMO1*) as regulated in both NS and COs. Furthermore, in the COs, the genes farnesyl-diphosphate

farnesyltransferase 1 (*FDFT1*), 7-dehydrocholesterol reductase (*DHCR7*) and 24-dehydrocholesterol reductase (*DHCR24*) were found to be differentially regulated (Figure 7B,C). We validated these findings for the genes *HMGCR*, *SQLE*, *DHCR7* and *MSMO1* via RT-qPCR (Figure 7D–K).

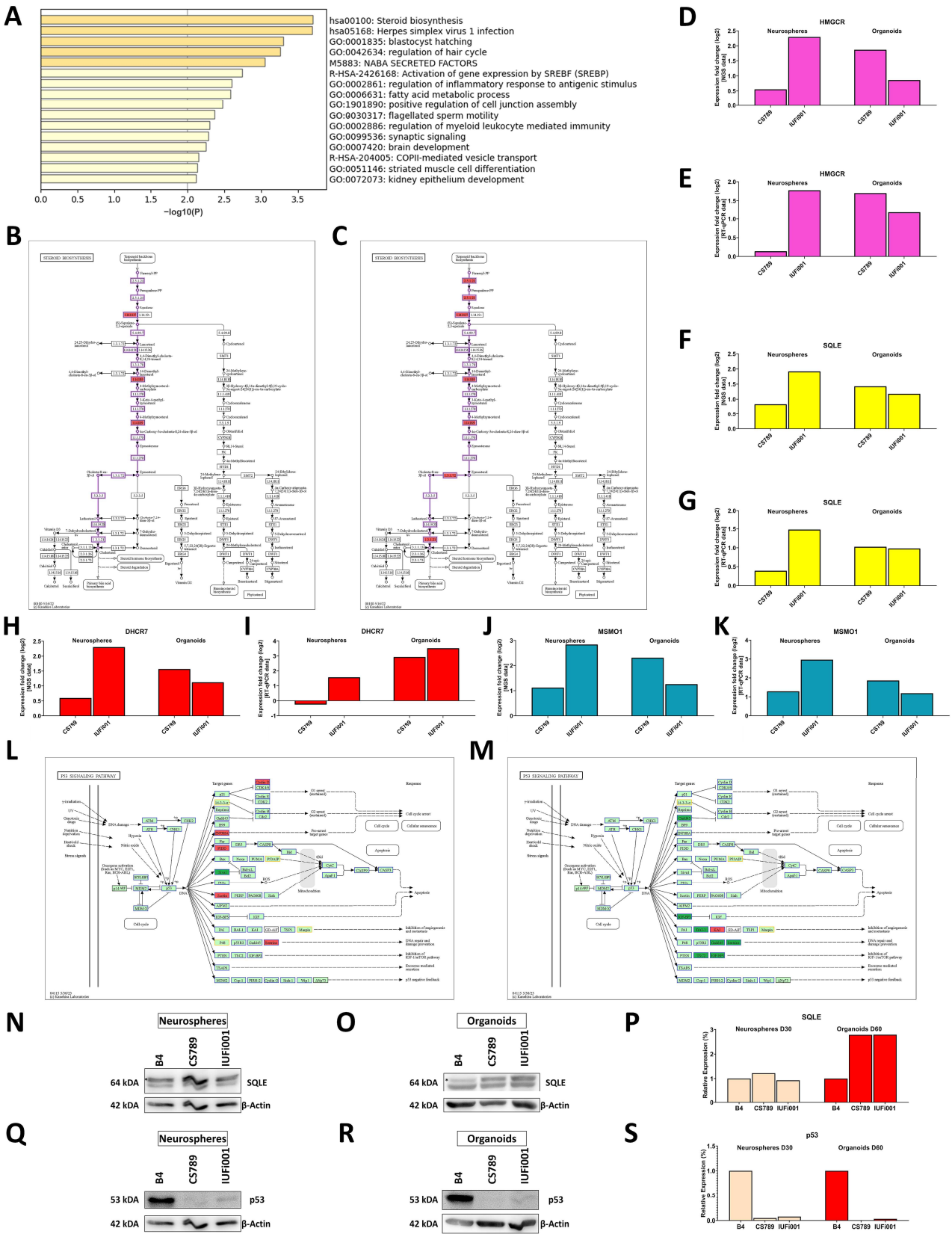

Figure 7. Metascape-based analysis of common genes dysregulated in day 30 CS neurospheres and day CS 60 organoids. (**A**) Bar graph of the 16 enrichment clusters attributable to the 181 DEGs

regulated in both day 30 CS NS and day 60 CS COs in comparison to CTRL (B4). (**B**,**C**) Schematic of the pathway steroid biosynthesis with the genes upregulated in CSB-deficient day 30 NS (**B**) and day 60 COs (**C**) indicated in red. (**D**,**F**,**H**,**J**) Relative mRNA expression analysis of *HMGCR* (**D**), *SQLE* (**F**), *DHCR7* (**H**) and *MSMO1* (**J**) in CS789 and IUFi001 organoids compared to CTRL (B4). (**E**,**G**,**I**,**K**) qRT-PCR analysis of *HMGCR* (**E**), *SQLE* (**G**), *DHCR7* (**I**) and *MSMO1* (**K**) mRNA expression in CS789 and IUFi001 organoids relative to CTRL (B4). (**L**,**M**) Schematic of p53 signalling pathway with genes upregulated in CSB-deficient day 30 NS (**L**) and day 60 COs (**M**) indicated in red and genes downregulated indicated in green. Genes which are not expressed are indicated in yellow. (**N**,**O**) Western blot analysis for SQLE in day 30 NS (**N**) and day 60 COs (**O**). (**P**) Quantification of SQLE Western blot analysis at the day 30 NS and day 60 CO stage in CTRL (B4), CS789 and IUFi001. SQLE expression of CS789 and IUFi001 is compared to SQLE expression in CTRL (B4) of the respective timepoint. (**Q**,**R**) Western blot analysis for p53 in day 30 NS (**Q**) and day 60 COs (**R**). (**S**) Quantification of p53 Western blot analysis at the day 30 NS and day 60 CO stage in CTRL (B4), CS789 and IUFi001. SQLE expression of CS789 and IUFi001 is compared to p53 expression in CTRL (B4) of the respective timepoint. (**N,O**) Asterisks (*) indicate bands of interest.

We further analysed whether the regulation of *SQLE* translated to an increase in protein levels via Western blot. We found no difference in the NS but a nearly threefold increase of SQLE in the COs (Figure 7N–P). The full Western blots can be found in Supplementary Figure S3.

Next, we analysed a pathway known to be dysregulated in CSB-deficient cells, the p53 signalling pathway. In the NS, we found the upregulation of zinc finger protein 385A (*ZNF385A*), P53-induced death domain protein 1 (*PIDD1*), shisa family member 5 (*SHISA5*), cyclin D1 (*CCND1*), sestrin 2 (*SESN2*) and sestrin 3 (*SESN3*), as well as the downregulation of SIVA1 apoptosis-inducing factor (*SIVA1*). In the COs, we found the downregulation of growth arrest and dNA-damage-inducible gamma (*GADD45G*), insulin-like growth factor binding protein 3 (*IGFBP3*), adhesion G protein-coupled receptor B1 (*ADGRB1*), *SESN2* and TSC complex subunit 2 (*TSC2*) as well as the upregulation of CD82 molecule (*CD82*) (Figure 7L,M). We further analysed the quantity of the p53 protein at both timepoints. Contrary to our expectations, we detected a decrease in p53 protein levels at both timepoints (Figure 7Q–S). The full Western Blots can be found in Supplementary Figure S3.

These results indicate the upregulation of CB during the early cerebral development of patients with CS. While we could identify the transcriptional upregulation of genes involved in CB in both day 30 NS and day 60 COs, this upregulation could only be confirmed on the translational level in the COs. Our results also confirm the dysregulation of the p53 signalling pathway in iPSC-derived NPCs and neurons during early human BD in patients with CS. Interestingly, this disruption of the p53 signalling pathway manifests in the altered expression of different genes between day 30 NS and day 60 COs. Unexpectedly, we detected a decrease in p53 protein levels at both timepoints.

4. Discussion

The major diagnostic criteria of CS are mostly symptoms of the central nervous system, e.g., progressive microcephaly, neurologic dysfunction and cerebellar atrophy. However, the mechanisms underlying these manifestations are still largely unknown due to the versatility of the causative protein and limitations of the available experimental models. To overcome this deficiency, we produced the first successful differentiation of CSB-deficient iPSC lines into cerebral organoids (COs). These COs enable us to model early developmental dysregulation in patients with CS and the effect of CSB deficiency on neural progenitor cells and neurons. The established model, however, does not include vascular cells or oligodendrocytes and is thus unable to reproduce neurological manifestations like hypomyelination and the dystrophic mineralization of vessels found in the central nervous system of patients with CS.

We employed two distinct, patient-derived, CSB-deficient iPSC lines, one generated from a donor with the most severe form of CS, cerebro-oculo-fascio-skeletal syndrome

(COFS), and one generated from a donor with classical CS type I and differentiated them into neural progenitor cells (NPCs), in the form of neurospheres (NS) and COs. To elucidate the common dysregulation underlying aberrations in brain development (BD) found in different types of CS, we then subjected the mRNA of both developmental timepoints, day 30 NS and day 60 COs, to NGS and the resulting datasets to extensive bioinformatic analysis. The transcriptome of day 30 NS is estimated to correspond to 8–9 week post-conception foetal brains and the transcriptome of day 60 COs to 13–21 week post-conception foetal brains [33,50]. COs produced with this protocol have been shown to consist mostly of cells with forebrain identity. However, sub-populations of cells with midbrain and hindbrain identity are to be expected [33,51].

Transcriptome-based analysis of the differentially regulated KEGG pathways in the NS revealed several common pathways. The upregulated pathway *protein processing in endoplasmatic reticulum* and the downregulated pathway *ribosome* could indicate changes in the translational priming of NPCs. Ribosome biogenesis has been shown to be impaired in CSA- and CSB-deficient cells before due to a disturbance of RNA polymerase I transcription and the processing of pre-rRNA [52,53]. A decrease in ribosome-related genes would be expected to result in a decrease in protein processing. This might indicate a compensatory mechanism to increase global protein production. However, it could also indicate the dysregulation of global protein synthesis, which has been implicated in the disease progression of schizophrenia patients [54].

Furthermore, our analysis indicated the *VEGFA-VEGFR2 signalling pathway* as modulated in our patient-derived cell lines. While known for its function in angiogenesis, VEGFA also has a direct impact on NPCs and neurons. VEGFA has been shown to increase the proliferation of primary embryonic cortical NPCs [55,56]. VEGFA has also been shown to decrease apoptosis in adult NPCs and to promote neuronal survival [57–61]. Additionally, VEGFA is surmised to be involved in dendrite outgrowth and axon guidance, two processes we found regulated in day 60 COs [56,58]. Overall, this increase in VEGFA-VEGFR2 signalling might present a compensatory mechanism to increase proliferation, which has been shown to be reduced in CSB-deficient NPCs [62] or a protective response to increased ambient stress, which can be observed in the form of *cellular responses to stress*.

We also provide an in-depth analysis of several regulated enrichment clusters in our patient-derived NS via heatmap analysis, namely, *vesicle-mediated transport*, *intracellular protein transport* and *head development*. Vesicular transport is an essential process by which membrane-bound vesicles are released from a donor compartment and transported to a specific cellular location. Disturbances of vesicle-mediated transport cause a multitude of disorders, several of which share symptoms with CS [63]. The following genes identified as regulated in our dataset have been associated with diseases caused by alterations in vesicle-mediated transport: LMAN1, SEC23A, SEC23B, SEC24B, SEC31A, GAK, VPS35L, DNM2, SBF1, BLOC1S1, COG1, COG4, SCYL1, MTM1, AP1S2, DENND5A and TRAPPC9 [64]. The dysregulation of a subpathway, namely COPII-mediated vesicle transport, is also observable between both investigated timepoints.

We were further interested in the GO *head development*. The observed upregulation of BD it encompasses could indicate a premature entry of NPCs into neurogenesis, a hallmark of microcephaly. One reason for this premature shift could be the increase in ambient cell stress observed in our analysis as DNA damage can promote accelerated neurogenesis [33,65–67]. Interestingly, patients with CS, except for patients with COFS, do not present microcephaly in prenatal development. Still, both of our patient-derived cell lines display similar regulation of BD at the NPC stage, indicating potential issues with developmental timing.

The highest upregulated KEGG pathway in day 60 COs, *steroid biosynthesis*, shows common dysregulation over both timepoints. *Steroid biosynthesis*, as well as the commonly dysregulated Reactome set *activation of gene expression by SREBF (SREBP)*, both encompass cholesterol biosynthesis (CB). Cholesterol is produced by neurons at early stages of BD. Cholesterol is necessary for the control of membrane fluidity and lipid raft structure and

influences, e.g., neuronal receptor activity [68–70]. Correctly orchestrated CB is essential for BD and directly influences pathways dysregulated in our CSB-deficient lines as cholesterol is involved in synaptogenesis, stability and recycling of synaptic neurotransmitters and neurite outgrowth [69,71–74]. Cholesterol depletion, as well as accumulation, can lead to neuronal dysfunction and ultimately to neurodegeneration [73,75]. In a mouse model with a conditional knock-out of CB in radial glia cells, the affected pups exhibited a progressive loss of cortical neurons, as well as postnatal proliferation and migration deficits of cerebellar granule precursors [76]. Overall, diseases of cholesterol metabolism have a high overlap of symptoms with CS, with many manifesting with i.a. neurological symptoms like psycho-motor impairment developmental delay and microcephaly [77].

We verified this upregulation of CB in the COs via RT-qPCR of the two rate-limiting enzymes *HMGCR* and *SQLE*, as well as *DHCR7* and *MSMO1*. On the protein level, we could detect a nearly 3-fold increase in the SQLE protein, reinforcing the hypothesis that CB is increased in CSB-deficient young neurons. Interestingly, while we could also detect an increase in *SQLE* transcription in our NS, this did not translate into an increase in the SQLE protein. However, NPCs react differently to cholesterol depletion than neurons. In a mouse model with a conditional FDFT1 knock-out in VZ-NPCs, VEGF expression via a hypoxia-inducible factor-1 independent pathway was strongly upregulated. This increased angiogenesis and thus the influx of external cholesterol to the NPCs [78]. Fittingly, we also identified the upregulation of the VEGFA-VEGFR2 signalling pathway in our NS.

The p53 signalling pathway, reputed in its role as a tumour suppressor and its function in DNA damage response, cell cycle arrest, senescence and apoptosis, is also involved in BD. The deletion, mutation and inhibition of p53 can lead to female-biased neural tube defects [79]. However, deletions of effectors of p53 can lead to various brain malformations [80]. Due to the variety of potential outcomes, it is surmised that p53 stabilization has a controlled, dose- and time-dependent effect on distinct cell types during development [79]. In the context of CS, CSA and CSB have been shown to interact with p53 and regulate its degradation. Both proteins form a complex with p53 and MDM2, which facilitates ubiquitination and the subsequent degradation of p53 in an MDM2-dependent manner [81]. Due to decreased degradation, CSA- and CSB-deficient cells show elevated levels of p53 [82]. CSB also interacts directly with p53, competing with the essential factor E1A binding protein p300 (EP300) for its binding site. As CSB has a higher affinity for p53, this negatively modulates the function of p53 [83–85]. In summary, the regulation of the p53 signalling pathway was expected, due to a decrease in the degradation of p53 and absence of a negative regulator of p53 activity. This might have implications for BD as p53 is involved in the proliferation and differentiation of NPCs [86], and a controlled dose- and time-dependent stabilization of p53 is necessary for correct development.

Surprisingly, instead of the expected increase, we detected a decrease in the p53 protein levels at both timepoints. p53 protein levels have been revealed to be high during early embryogenesis and to decrease over the course of development until it plateaus at a low level in terminally differentiated cells [87–89]. This decrease in p53 protein levels we identified might be another manifestation of the dysregulation of BD we revealed in this work, further uncoupling the development of our CS-deficient cells from normal cerebral development. Another possibility would be the increased modification of p53, depleting the pool of unmodified p53 we examined, which would also directly impact BD.

The most significantly downregulated KEGG pathway in both patient-derived COs, *axon guidance*, has been shown to be dysregulated in human neuronal networks, as well as *axonogenesis*, which shows, in our analysis, as subpathway of *neuron projection development* [27]. In human neural cell lines, the ablation of CSB expression affected neuronal differentiation capabilities. The suppression of CSB led to a decrease in MAP2 expression, accompanied by reduced cell polarization. Together, this led to a decrease in neuritogenesis [16,90]. Alterations of neuritogenesis and axonal pathfinding may lead to pathological changes in neural circuitry.

The downregulated KEGG pathway *synaptic vesicle cycle* has been demonstrated to be dysregulated, as well as other pathways involved in synapse formation, activity and maintenance, whose dysregulation we could observe with the regulated *GOs regulation of trans-synaptic signalling*, *regulation of synapse structure* and *synaptic signalling* [27]. The correct function of synapse pathways are necessary for neuronal function and signal transmission, which both have been shown to be altered in CSB-deficient neural networks [27]. In CS patient cerebella, the downregulation of genes involved in synaptic exocytosis has been identified, which we also identified in our COs [16]. Our data also indicate the downregulation of synaptic endocytosis in our patient-derived COs. This alteration of synapse formation, activity and maintenance and the resulting changes likely contribute to the neurodevelopmental defects in patients with CS.

We further provide an analysis of several regulated enrichment clusters in our patient-derived COs via heatmap analysis, namely, the GOs *neuron projection development*, *synaptic signalling* and *brain development*.

Brain development, which was upregulated in NS, was found to be downregulated in day 60 COs. This was expected as CSB-deficient cells have been shown to exhibit the downregulation of thousands of genes, including brain-related genes, due to dysregulation of RNA polymerase II activity [15,16]. We found the brain development-related genes EPHA7, EPHB3, AFF2, NPY, WNT7B, TSPAN2, SRGAP2, UFM1, FUT10, POTEE, TRH and TPGS1 to be mostly upregulated in NS and downregulated in COs at both investigated timepoints.

However, the most significantly dysregulated genes are not associated with brain development. We found the genes *MAGEA4*, *TMEM132C*, *ZNF558* and *TRIM4* to be most severely regulated in all patient-derived samples. Other members of the MAGE-A family have been shown to potentially be involved in early BD [91]. *TMEM132C* has been revealed to be expressed in early NPCs and the developing cochlea and is differentially regulated in the dorsal forebrain and midbrain during murine development [92]. *TMEM132C* has also been shown to be differentially regulated in the NPCs of another disease with congenital cataracts and intellectual disability, Lowe syndrome [93]. Krüppel-associated box (KRAB) zinc finger protein *ZNF558*, has a role in mitochondrial maintenance and is thought to influence timing during early human BD [94]. *TRIM4* is a gene mainly known for its role in the ubiquitination of a variety of targets [95–97]. A genome-wide DNA methylation study found that the upregulation of *TRIM4* might be associated with neural tube defects [98].

So, while these four genes are not yet conclusively linked to BD, one can assume they might be associated. Interestingly, this dysregulation of all four genes seems to be traceable to later timepoints, indicating their involvement not only in early but at least also in mid-gestational BD.

To further decipher CS and find target genes utilizable in all forms of CS, a comparison between CSA- and CSB-deficient cerebral organoids is crucial. A comparison between CSA- and CSB-depleted SH-SY5Y cells showed significant overlap between the transcriptional dysregulation of both proteins but also regulation distinct to both. On the transcriptional and functional level, Wu et al. found CSB deficiency to inhibit neuritogenesis, while CSA deficiency even slightly increased the differentiation of the SH-SY5Y cells. This is a striking finding as patients with mutations in both genes show neurological symptoms and neurodegeneration [99]. As the symptoms of mutations in both proteins are largely convergent, but not identical, it would be interesting to identify the convergent and divergent mechanisms resulting in the subtle differences between both patient cohorts.

Due to the involvement of CSA and CSB in TC-NER, there has been an ongoing debate whether CS is a neurodegenerative or neurodevelopmental disorder. This work only concentrates on the neurodevelopmental effects of CS as we did not challenge the TC-NER via UV radiation or pharmacological intervention. We therefore expect the endogenous lesions warranting TC-NER to be menial. Nonetheless, the differences at steady-state are already sizeable, with the dysregulation of ribosome-related pathways in NPCs and the

disruption of several pathways crucial for neuronal function and survival on the transcriptional level. Our findings are in line with a proposed hypothesis characterizing CS as a transcription syndrome, with many of the especially neurological symptoms being caused mainly by the dysregulation of RNAPI and RNAPII transcription rather than the inactivation of TC-NER [100].

5. Conclusions

In conclusion, this study is the first to produce CSB-deficient patient-derived 3D organoids. Our data provide new insights into the transcriptional dysregulation associated with brain development in patients with CS. We confirm the known dysregulation of neuron projection- and synapse-related pathways and expand this set with the dysregulation of the metabolic pathway steroid biosynthesis, as well as the dysregulation of lipid metabolism in NPCs and neurons in a 3D environment. Our data further provide substantiation to the theory that CS is not only a neurodegenerative but also a neurodevelopmental disorder, with a characteristic dysregulation of brain development at distinct stages. We also identified highly differentially regulated genes not previously highlighted in CSB-deficient neuronal cultures. These genes seem to be dysregulated at several stages of brain development, indicating them as potential target candidates for intervention.

Sadly, due to the rarity of CS and experimental limitations, only a small cohort was investigated. This increases the chance of a false-positive identification of differences. To mitigate this issue, future investigations should include more CS and control individuals, as well as optimally a CRISPR/Cas-mediated rescue of at least one CS cell line. Still, this work strengthens already established theories about the aetiology of CS and might provide leads for further research. As a future prospect, a deeper understanding of the underlying developmental dysregulation in the most devastating symptoms of CS can hopefully spur the development of therapeutic strategies.

Supplementary Materials: The following supporting information can be downloaded at: https://www.mdpi.com/article/10.3390/cells13070591/s1, Figure S1: Used cell lines and clinical information about Cockayne syndrome; Figure S2: Determination of developmental age of day 30 neurospheres and day 60 cortical organoids; Figure S3: Full Western blot for CSB, SQLE, p53 and beta-actin protein in Day 0 iPSCs, Day 30 NS and Day 60 COs; Figure S4: Quality control of next-generation sequencing data; Figure S5: Global transcriptome and associated gene ontology analysis of control and CS neurospheres on day 30; Figure S6: Comparative transcriptome and gene ontology analysis of downregulated DEGs in day 30 neurospheres; Figure S7: Analysis of select gene ontologies differentially regulated in day 30 neurospheres; Figure S8: Global transcriptome and associated gene ontology analysis of control and CS organoids on day 60; Figure S9: Comparative transcriptome and gene ontology analysis of upregulated DEGs in day 60 organoids; Figure S10: Analysis of select gene ontologies differentially regulated in day 60 organoids; Figure S11: RT-qPCR for MAGEA4, TMEM132C, ZNF558 and TRIM4 in Day 30 neurospheres, two sets of day 60 organoids and day 120 organoids; Figure S12: Analysis of the mevalonate pathway of the terpenoid backbone biosynthesis pathway in day 30 NS and day 60 COs; Supplementary Table S1: Primers and antibodies; Supplementary Table S2: Top 50 KEGG lists.

Author Contributions: Conceptualisation, J.A., J.K. (Jean Krutmann), E.F. and L.-P.S.; formal analysis, L.-P.S. and W.W.; investigation, L.-P.S., W.W., A.R. and J.K. (Julia Kapr); resources, J.A., J.K. (Jean Krutmann), E.F., A.R. and J.K. (Julia Kapr); data curation, L.-P.S. and W.W. ; writing—original draft preparation, L.-P.S.; writing—review and editing, J.A. and W.W.; visualization, L.-P.S. and W.W.; supervision, J.A.; project administration, J.A., J.K. (Jean Krutmann) and E.F.; funding acquisition, J.A., J.K. (Jean Krutmann) and E.F. All authors have read and agreed to the published version of the manuscript.

Funding: This work was funded by the medical faculty of Heinrich Heine University Düsseldorf, the Leibniz Association (project-number K246/2019) and the German Research Foundation (project-number 417677437/GRK2578 "Impact of genotoxins on the differentiation efficacy of murine and human stem and progenitor cells and functional competence of thereof derived differentiated progeny"; Sub-project: 1a.)

Institutional Review Board Statement: The study was conducted in accordance with the Declaration of Helsinki, and approval for the use of iPSC lines was granted by the ethics committee of the medical faculty of Heinrich Heine University Duesseldorf (study number 5013, approved 9 June 2015).

Informed Consent Statement: Not applicable.

Data Availability Statement: The RNA-Seq datasets generated and analysed during the current study will be made available on NCBI GEO after the manuscript is accepted in a journal.

Acknowledgments: The authors are grateful to Kanehisa Laboratories for the permission to use their figures for terpenoid backbone biosynthesis, steroid biosynthesis and p53 signalling pathways for our figures. The figures were taken from https://www.genome.jp/kegg/(accessed on 16 June 2023).

Conflicts of Interest: The authors declare no conflicts of interest. The funders had no role in the design of the study; in the collection, analyses or interpretation of data; in the writing of the manuscript; or in the decision to publish the results.

References

1. Cockayne, E.A. Dwarfism with retinal atrophy and deafness. *Arch. Dis. Child.* **1936**, *11*, 1.
2. Licht, C.L.; Stevnsner, T.; Bohr, V.A. Cockayne syndrome group B cellular and biochemical functions. *Am. J. Hum. Genet.* **2003**, *73*, 1217–1239.
3. Nance, M.A.; Berry, S.A. Cockayne syndrome: Review of 140 cases. *Am. J. Med. Genet.* **1992**, *42*, 68–84.
4. Laugel, V. Cockayne syndrome: The expanding clinical and mutational spectrum. *Mech. Ageing Dev.* **2013**, *134*, 161–170. https://doi.org/10.1016/j.mad.2013.02.006.
5. Weidenheim, K.M.; Dickson, D.W.; Rapin, I. Neuropathology of Cockayne syndrome: Evidence for impaired development, premature aging, and neurodegeneration. *Mech. Ageing Dev.* **2009**, *130*, 619–636.
6. Marteijn, J.A.; Lans, H.; Vermeulen, W.; Hoeijmakers, J.H. Understanding nucleotide excision repair and its roles in cancer and ageing. *Nat. Rev. Mol. Cell Biol.* **2014**, *15*, 465–481. https://doi.org/10.1038/nrm3822.
7. Gupta, S.; You, P.; SenGupta, T.; Nilsen, H.; Sharma, K. Crosstalk between different DNA repair pathways contributes to neurodegenerative diseases. *Biology* **2021**, *10*, 163.
8. Muftuoglu, M.; de Souza-Pinto, N.C.; Dogan, A.; Aamann, M.; Stevnsner, T.; Rybanska, I.; Kirkali, G.; Dizdaroglu, M.; Bohr, V.A. Cockayne syndrome group B protein stimulates repair of formamidopyrimidines by NEIL1 DNA glycosylase. *J. Biol. Chem.* **2009**, *284*, 9270–9279.
9. Thorslund, T.; von Kobbe, C.; Harrigan, J.A.; Indig, F.E.; Christiansen, M.; Stevnsner, T.; Bohr, V.A. Cooperation of the Cockayne syndrome group B protein and poly (ADP-ribose) polymerase 1 in the response to oxidative stress. *Mol. Cell. Biol.* **2005**, *25*, 7625–7636.
10. Wong, H.-K.; Muftuoglu, M.; Beck, G.; Imam, S.Z.; Bohr, V.A.; Wilson III, D.M. Cockayne syndrome B protein stimulates apurinic endonuclease 1 activity and protects against agents that introduce base excision repair intermediates. *Nucleic Acids Res.* **2007**, *35*, 4103–4113.
11. Tiwari, V.; Baptiste, B.A.; Okur, M.N.; Bohr, V.A. Current and emerging roles of Cockayne syndrome group B (CSB) protein. *Nucleic Acids Res.* **2021**, *49*, 2418–2434. https://doi.org/10.1093/nar/gkab085.
12. Batenburg, N.L.; Thompson, E.L.; Hendrickson, E.A.; Zhu, X.D. Cockayne syndrome group B protein regulates DNA double-strand break repair and checkpoint activation. *EMBO J.* **2015**, *34*, 1399–1416. https://doi.org/10.15252/embj.201490041.
13. Iyama, T.; Lee, S.Y.; Berquist, B.R.; Gileadi, O.; Bohr, V.A.; Seidman, M.M.; McHugh, P.J.; Wilson, D.M., 3rd. CSB interacts with SNM1A and promotes DNA interstrand crosslink processing. *Nucleic Acids Res.* **2015**, *43*, 247–258. https://doi.org/10.1093/nar/gku1279.
14. Iyama, T.; Wilson, D.M., 3rd. Elements That Regulate the DNA Damage Response of Proteins Defective in Cockayne Syndrome. *J. Mol. Biol.* **2016**, *428*, 62–78. https://doi.org/10.1016/j.jmb.2015.11.020.
15. Balajee, A.S.; May, A.; Dianov, G.L.; Friedberg, E.C.; Bohr, V.A. Reduced RNA polymerase II transcription in intact and permeabilized Cockayne syndrome group B cells. *Proc. Natl. Acad. Sci. USA* **1997**, *94*, 4306–4311.
16. Wang, Y.; Chakravarty, P.; Ranes, M.; Kelly, G.; Brooks, P.J.; Neilan, E.; Stewart, A.; Schiavo, G.; Svejstrup, J.Q. Dysregulation of gene expression as a cause of Cockayne syndrome neurological disease. *Proc. Natl. Acad. Sci. USA* **2014**, *111*, 14454–14459.
17. van der Horst, G.T.; van Steeg, H.; Berg, R.J.; van Gool, A.J.; de Wit, J.; Weeda, G.; Morreau, H.; Beems, R.B.; van Kreijl, C.F.; de Gruijl, F.R. Defective transcription-coupled repair in Cockayne syndrome B mice is associated with skin cancer predisposition. *Cell* **1997**, *89*, 425–435.
18. Van Der Horst, G.T.; Meira, L.; Gorgels, T.G.; De Wit, J.; Velasco-Miguel, S.; Richardson, J.A.; Kamp, Y.; Vreeswijk, M.P.; Smit, B.; Bootsma, D. UVB radiation-induced cancer predisposition in Cockayne syndrome group A (Csa) mutant mice. *DNA Repair* **2002**, *1*, 143–157.

19. Jaarsma, D.; van der Pluijm, I.; van der Horst, G.T.; Hoeijmakers, J.H. Cockayne syndrome pathogenesis: Lessons from mouse models. *Mech. Ageing Dev.* **2013**, *134*, 180–195.
20. Andressoo, J.-O.; Weeda, G.; de Wit, J.; Mitchell, J.R.; Beems, R.B.; van Steeg, H.; van der Horst, G.T.; Hoeijmakers, J.H. An Xpb mouse model for combined xeroderma pigmentosum and cockayne syndrome reveals progeroid features upon further attenuation of DNA repair. *Mol. Cell. Biol.* **2009**, *29*, 1276–1290.
21. Andressoo, J.-O.; Mitchell, J.R.; de Wit, J.; Hoogstraten, D.; Volker, M.; Toussaint, W.; Speksnijder, E.; Beems, R.B.; van Steeg, H.; Jans, J. An Xpd mouse model for the combined xeroderma pigmentosum/Cockayne syndrome exhibiting both cancer predisposition and segmental progeria. *Cancer Cell* **2006**, *10*, 121–132.
22. Harada, Y.-N.; Shiomi, N.; Koike, M.; Ikawa, M.; Okabe, M.; Hirota, S.; Kitamura, Y.; Kitagawa, M.; Matsunaga, T.; Nikaido, O. Postnatal growth failure, short life span, and early onset of cellular senescence and subsequent immortalization in mice lacking the xeroderma pigmentosum group G gene. *Mol. Cell. Biol.* **1999**, *19*, 2366–2372.
23. Karikkineth, A.C.; Scheibye-Knudsen, M.; Fivenson, E.; Croteau, D.L.; Bohr, V.A. Cockayne syndrome: Clinical features, model systems and pathways. *Ageing Res. Rev.* **2017**, *33*, 3–17. https://doi.org/10.1016/j.arr.2016.08.002.
24. Andrade, L.N.d.S.; Nathanson, J.L.; Yeo, G.W.; Menck, C.F.M.; Muotri, A.R. Evidence for premature aging due to oxidative stress in iPSCs from Cockayne syndrome. *Hum. Mol. Genet.* **2012**, *21*, 3825–3834.
25. Kristensen, U.; Epanchintsev, A.; Rauschendorf, M.-A.; Laugel, V.; Stevnsner, T.; Bohr, V.A.; Coin, F.; Egly, J.-M. Regulatory interplay of Cockayne syndrome B ATPase and stress-response gene ATF3 following genotoxic stress. *Proc. Natl. Acad. Sci. USA* **2013**, *110*, E2261–E2270.
26. Wang, Y.; Jones-Tabah, J.; Chakravarty, P.; Stewart, A.; Muotri, A.; Laposa, R.R.; Svejstrup, J.Q. Pharmacological bypass of Cockayne syndrome B function in neuronal differentiation. *Cell Rep.* **2016**, *14*, 2554–2561.
27. Vessoni, A.T.; Herai, R.H.; Karpiak, J.V.; Leal, A.M.; Trujillo, C.A.; Quinet, A.; Agnez Lima, L.F.; Menck, C.F.; Muotri, A.R. Cockayne syndrome-derived neurons display reduced synapse density and altered neural network synchrony. *Hum. Mol. Genet.* **2016**, *25*, 1271–1280.
28. Wang, S.; Min, Z.; Ji, Q.; Geng, L.; Su, Y.; Liu, Z.; Hu, H.; Wang, L.; Zhang, W.; Suzuiki, K. Rescue of premature aging defects in Cockayne syndrome stem cells by CRISPR/Cas9-mediated gene correction. *Protein Cell* **2020**, *11*, 1–22.
29. Kapr, J.; Petersilie, L.; Distler, T.; Lauria, I.; Bendt, F.; Sauter, C.M.; Boccaccini, A.R.; Rose, C.R.; Fritsche, E. Human Induced Pluripotent Stem Cell-Derived Neural Progenitor Cells Produce Distinct Neural 3D In Vitro Models Depending on Alginate/Gellan Gum/Laminin Hydrogel Blend Properties. *Adv. Healthc. Mater.* **2021**, *10*, 2100131.
30. Martins, S.; Hacheney, I.; Teichweyde, N.; Hildebrandt, B.; Krutmann, J.; Rossi, A. Generation of an induced pluripotent stem cell line (IUFi001) from a Cockayne syndrome patient carrying a mutation in the ERCC6 gene. *Stem Cell Res.* **2021**, *55*, 102456.
31. Hofrichter, M. Establishment of a hiPSC-Based In Vitro Model to Study Environmental and Genetic Disturbances of Neurodevelopmental Processes. Inaugural-Dissertation, Heinrich-Heine-Universität Düsseldorf, Düsseldorf, Germany, 2016.
32. Wang, Y.; Adjaye, J. A cyclic AMP analog, 8-Br-cAMP, enhances the induction of pluripotency in human fibroblast cells. *Stem Cell Rev. Rep.* **2011**, *7*, 331–341.
33. Martins, S.; Erichsen, L.; Datsi, A.; Wruck, W.; Goering, W.; Chatzantonaki, E.; de Amorim, V.C.M.; Rossi, A.; Chrzanowska, K.H.; Adjaye, J. Impaired p53-mediated DNA damage response contributes to microcephaly in Nijmegen Breakage Syndrome patient-derived cerebral organoids. *Cells* **2022**, *11*, 802.
34. Martins, S.; Müller-Schiffmann, A.; Erichsen, L.; Bohndorf, M.; Wruck, W.; Sleegers, K.; Van Broeckhoven, C.; Korth, C.; Adjaye, J. IPSC-derived neuronal cultures carrying the Alzheimer's disease associated TREM2 R47H variant enables the construction of an Aβ-induced gene regulatory network. *Int. J. Mol. Sci.* **2020**, *21*, 4516.
35. Sloan, S.A.; Andersen, J.; Pasca, A.M.; Birey, F.; Pasca, S.P. Generation and assembly of human brain region-specific three-dimensional cultures. *Nat. Protoc.* **2018**, *13*, 2062–2085. https://doi.org/10.1038/s41596-018-0032-7.
36. Liu, Y.; Liu, H.; Sauvey, C.; Yao, L.; Zarnowska, E.D.; Zhang, S.-C. Directed differentiation of forebrain GABA interneurons from human pluripotent stem cells. *Nat. Protoc.* **2013**, *8*, 1670–1679.
37. Kim, D.; Langmead, B.; Salzberg, S.L. HISAT: A fast spliced aligner with low memory requirements. *Nat. Methods* **2015**, *12*, 357–360.
38. Gentleman, R.C.; Carey, V.J.; Bates, D.M.; Bolstad, B.; Dettling, M.; Dudoit, S.; Ellis, B.; Gautier, L.; Ge, Y.; Gentry, J. Bioconductor: Open software development for computational biology and bioinformatics. *Genome Biol.* **2004**, *5*, R80.
39. Chen, H.; Boutros, P.C. VennDiagram: A package for the generation of highly-customizable Venn and Euler diagrams in R. *BMC Bioinform.* **2011**, *12*, 35.
40. Warnes, M.G.R.; Bolker, B.; Bonebakker, L.; Gentleman, R.; Huber, W.; Liaw, A. Package 'gplots'. In *Various R Programming Tools for Plotting Data*; R Foundation for Statistical Computing: Vienna, Austria, 2016.
41. Falcon, S.; Gentleman, R. Using GOstats to test gene lists for GO term association. *Bioinformatics* **2007**, *23*, 257–258.
42. Kanehisa, M.; Furumichi, M.; Tanabe, M.; Sato, Y.; Morishima, K. KEGG: New perspectives on genomes, pathways, diseases and drugs. *Nucleic Acids Res.* **2017**, *45*, D353–D361.
43. Kanehisa, M.; Goto, S. KEGG: Kyoto encyclopedia of genes and genomes. *Nucleic Acids Res.* **2000**, *28*, 27–30.
44. Kanehisa, M. Toward understanding the origin and evolution of cellular organisms. *Protein Sci.* **2019**, *28*, 1947–1951.
45. Kanehisa, M.; Furumichi, M.; Sato, Y.; Kawashima, M.; Ishiguro-Watanabe, M. KEGG for taxonomy-based analysis of pathways and genomes. *Nucleic Acids Res.* **2023**, *51*, D587–D592.
46. Wickham, H. *ggplot2: Elegant Grophics for Data Analysis*; Springer: New York, NY, USA, 2009.

47. Zhou, Y.; Zhou, B.; Pache, L.; Chang, M.; Khodabakhshi, A.H.; Tanaseichuk, O.; Benner, C.; Chanda, S.K. Metascape provides a biologist-oriented resource for the analysis of systems-level datasets. *Nat. Commun.* **2019**, *10*, 1523.
48. Jones, A.R.; Overly, C.C.; Sunkin, S.M. The Allen brain atlas: 5 years and beyond. *Nat. Rev. Neurosci.* **2009**, *10*, 821–828.
49. Hänzelmann, S.; Castelo, R.; Guinney, J. GSVA: Gene set variation analysis for microarray and RNA-seq data. *BMC Bioinform.* **2013**, *14*, 7.
50. Miller, J.A.; Ding, S.-L.; Sunkin, S.M.; Smith, K.A.; Ng, L.; Szafer, A.; Ebbert, A.; Riley, Z.L.; Royall, J.J.; Aiona, K. Transcriptional landscape of the prenatal human brain. *Nature* **2014**, *508*, 199–206.
51. Lancaster, M.A.; Renner, M.; Martin, C.-A.; Wenzel, D.; Bicknell, L.S.; Hurles, M.E.; Homfray, T.; Penninger, J.M.; Jackson, A.P.; Knoblich, J.A. Cerebral organoids model human brain development and microcephaly. *Nature* **2013**, *501*, 373–379.
52. Qiang, M.; Khalid, F.; Phan, T.; Ludwig, C.; Scharffetter-Kochanek, K.; Iben, S. Cockayne syndrome-associated CSA and CSB mutations impair ribosome biogenesis, ribosomal protein stability, and global protein folding. *Cells* **2021**, *10*, 1616.
53. Alupei, M.C.; Maity, P.; Esser, P.R.; Krikki, I.; Tuorto, F.; Parlato, R.; Penzo, M.; Schelling, A.; Laugel, V.; Montanaro, L. Loss of proteostasis is a pathomechanism in Cockayne syndrome. *Cell Rep.* **2018**, *23*, 1612–1619.
54. Topol, A.; English, J.; Flaherty, E.; Rajarajan, P.; Hartley, B.; Gupta, S.; Desland, F.; Zhu, S.; Goff, T.; Friedman, L. Increased abundance of translation machinery in stem cell–derived neural progenitor cells from four schizophrenia patients. *Transl. Psychiatry* **2015**, *5*, e662–e662.
55. Jin, K.; Zhu, Y.; Sun, Y.; Mao, X.O.; Xie, L.; Greenberg, D.A. Vascular endothelial growth factor (VEGF) stimulates neurogenesis in vitro and in vivo. *Proc. Natl. Acad. Sci. USA* **2002**, *99*, 11946–11950.
56. Mackenzie, F.; Ruhrberg, C. Diverse roles for VEGF-A in the nervous system. *Development* **2012**, *139*, 1371–1380.
57. Schänzer, A.; Wachs, F.P.; Wilhelm, D.; Acker, T.; Cooper-Kuhn, C.; Beck, H.; Winkler, J.; Aigner, L.; Plate, K.H.; Kuhn, H.G. Direct stimulation of adult neural stem cells in vitro and neurogenesis in vivo by vascular endothelial growth factor. *Brain Pathol.* **2004**, *14*, 237–248.
58. Rosenstein, J.M.; Mani, N.; Khaibullina, A.; Krum, J.M. Neurotrophic effects of vascular endothelial growth factor on organotypic cortical explants and primary cortical neurons. *J. Neurosci.* **2003**, *23*, 11036–11044.
59. Jin, K.L.; Mao, X.O.; Greenberg, D.A. Vascular endothelial growth factor: Direct neuroprotective effect in in vitro ischemia. *Proc. Natl. Acad. Sci. USA* **2000**, *97*, 10242–10247.
60. Cui, W.; Li, W.; Han, R.; Mak, S.; Zhang, H.; Hu, S.; Rong, J.; Han, Y. PI3-K/Akt and ERK pathways activated by VEGF play opposite roles in MPP+-induced neuronal apoptosis. *Neurochem. Int.* **2011**, *59*, 945–953.
61. Matsuzaki, H.; Tamatani, M.; Yamaguchi, A.; Namikawa, K.; Kiyama, H.; Vitek, M.P.; Mitsuda, N.; Tohyama, M. Vascular endothelial growth factor rescues hippocampal neurons from glutamate-induced toxicity: Signal transduction cascades. *FASEB J.* **2001**, *15*, 1218–1220.
62. Sacco, R.; Tamblyn, L.; Rajakulendran, N.; Bralha, F.N.; Tropepe, V.; Laposa, R.R. Cockayne syndrome b maintains neural precursor function. *DNA Repair* **2013**, *12*, 110–120.
63. Gissen, P.; Maher, E.R. Cargos and genes: Insights into vesicular transport from inherited human disease. *J. Med. Genet.* **2007**, *44*, 545–555.
64. Yarwood, R.; Hellicar, J.; Woodman, P.G.; Lowe, M. Membrane trafficking in health and disease. *Dis. Models Mech.* **2020**, *13*, dmm043448.
65. Li, R.; Sun, L.; Fang, A.; Li, P.; Wu, Q.; Wang, X. Recapitulating cortical development with organoid culture in vitro and modeling abnormal spindle-like (ASPM related primary) microcephaly disease. *Protein Cell* **2017**, *8*, 823–833.
66. Gabriel, E.; Wason, A.; Ramani, A.; Gooi, L.M.; Keller, P.; Pozniakovsky, A.; Poser, I.; Noack, F.; Telugu, N.S.; Calegari, F. CPAP promotes timely cilium disassembly to maintain neural progenitor pool. *EMBO J.* **2016**, *35*, 803–819.
67. Su, Y.; Ming, G.-l.; Song, H. DNA damage and repair regulate neuronal gene expression. *Cell Res.* **2015**, *25*, 993–994.
68. Segatto, M.; Di Giovanni, A.; Marino, M.; Pallottini, V. Analysis of the protein network of cholesterol homeostasis in different brain regions: An age and sex dependent perspective. *J. Cell. Physiol.* **2013**, *228*, 1561–1567.
69. Hussain, G.; Wang, J.; Rasul, A.; Anwar, H.; Imran, A.; Qasim, M.; Zafar, S.; Kamran, S.K.S.; Razzaq, A.; Aziz, N. Role of cholesterol and sphingolipids in brain development and neurological diseases. *Lipids Health Dis.* **2019**, *18*, 26.
70. Zuo, H.; Wang, R.; Jiang, D.; Fang, D. Determining the composition of active Cholesterol in the plasma membrane of single cells by using Electrochemiluminescence. *ChemElectroChem* **2017**, *4*, 1677–1680.
71. Goritz, C.; Mauch, D.H.; Pfrieger, F.W. Multiple mechanisms mediate cholesterol-induced synaptogenesis in a CNS neuron. *Mol. Cell. Neurosci.* **2005**, *29*, 190–201.
72. Adibhatla, R.M.; Hatcher, J. Altered lipid metabolism in brain injury and disorders. In *Lipids in Health and Disease*; Springer: Dordrecht, The Netherland, 2008; pp. 241–268.
73. Martín, M.G.; Pfrieger, F.; Dotti, C.G. Cholesterol in brain disease: Sometimes determinant and frequently implicated. *EMBO Rep.* **2014**, *15*, 1036–1052.
74. Mauch, D.H.; Nagler, K.; Schumacher, S.; Goritz, C.; Muller, E.-C.; Otto, A.; Pfrieger, F.W. CNS synaptogenesis promoted by glia-derived cholesterol. *Science* **2001**, *294*, 1354–1357.
75. Djelti, F.; Braudeau, J.; Hudry, E.; Dhenain, M.; Varin, J.; Bieche, I.; Marquer, C.; Chali, F.; Ayciriex, S.; Auzeil, N. CYP46A1 inhibition, brain cholesterol accumulation and neurodegeneration pave the way for Alzheimer's disease. *Brain* **2015**, *138*, 2383–2398.

76. Cunningham, D.; DeBarber, A.E.; Bir, N.; Binkley, L.; Merkens, L.S.; Steiner, R.D.; Herman, G.E. Analysis of hedgehog signaling in cerebellar granule cell precursors in a conditional Nsdhl allele demonstrates an essential role for cholesterol in postnatal CNS development. *Hum. Mol. Genet.* **2015**, *24*, 2808–2825.
77. Jira, P. Cholesterol metabolism deficiency. In *Handbook of Clinical Neurology*; Elsevier: Amsterdam, The Netherlands, 2013; Volume 113, pp. 1845–1850.
78. Saito, K.; Dubreuil, V.; Arai, Y.; Wilsch-Bräuninger, M.; Schwudke, D.; Saher, G.; Miyata, T.; Breier, G.; Thiele, C.; Shevchenko, A. Ablation of cholesterol biosynthesis in neural stem cells increases their VEGF expression and angiogenesis but causes neuron apoptosis. *Proc. Natl. Acad. Sci. USA* **2009**, *106*, 8350–8355.
79. Xiong, Y.; Zhang, Y.; Xiong, S.; Williams-Villalobo, A.E. A glance of p53 functions in brain development, neural stem cells, and brain cancer. *Biology* **2020**, *9*, 285.
80. Xiong, S.; Van Pelt, C.S.; Elizondo-Fraire, A.C.; Liu, G.; Lozano, G. Synergistic roles of Mdm2 and Mdm4 for p53 inhibition in central nervous system development. *Proc. Natl. Acad. Sci. USA* **2006**, *103*, 3226–3231.
81. Latini, P.; Frontini, M.; Caputo, M.; Gregan, J.; Cipak, L.; Filippi, S.; Kumar, V.; Vélez-Cruz, R.; Stefanini, M.; Proietti-De-Santis, L. CSA and CSB proteins interact with p53 and regulate its Mdm2-dependent ubiquitination. *Cell Cycle* **2011**, *10*, 3719–3730.
82. Jaarsma, D.; van der Pluijm, I.; de Waard, M.C.; Haasdijk, E.D.; Brandt, R.; Vermeij, M.; Rijksen, Y.; Maas, A.; van Steeg, H.; Hoeijmakers, J.H. Age-related neuronal degeneration: Complementary roles of nucleotide excision repair and transcription-coupled repair in preventing neuropathology. *PLoS Genet.* **2011**, *7*, e1002405.
83. Filippi, S.; Latini, P.; Frontini, M.; Palitti, F.; Egly, J.M.; Proietti-De-Santis, L. CSB protein is (a direct target of HIF-1 and) a critical mediator of the hypoxic response. *EMBO J.* **2008**, *27*, 2545–2556.
84. Proietti-De-Santis, L.; Laugel, V.; Prantera, G. Cockayne syndrome. In *Chromatin Signaling and Neurological Disorders*; Elsevier: Amsterdam, The Netherlands, 2019; pp. 135–152.
85. Frontini, M.; Proietti-De-Santis, L. Cockayne syndrome B protein (CSB): Linking p53, HIF-1 and p300 to robustness, lifespan, cancer and cell fate decisions. *Cell Cycle* **2009**, *8*, 693–696.
86. Armesilla-Díaz, A.; Bragado, P.; Del Valle, I.; Cuevas, E.; Lázaro, I.; Martin, C.; Cigudosa, J.; Silva, A. p53 regulates the self-renewal and differentiation of neural precursors. *Neuroscience* **2009**, *158*, 1378–1389.
87. Molchadsky, A.; Rivlin, N.; Brosh, R.; Rotter, V.; Sarig, R. p53 is balancing development, differentiation and de-differentiation to assure cancer prevention. *Carcinogenesis* **2010**, *31*, 1501–1508.
88. Louis, J.M.; McFarland, V.W.; May, P.; Mora, P.T. The phosphoprotein p53 is down-regulated post-transcriptionally during embryogenesis in vertebrates. *Biochim. Biophys. Acta (BBA)-Gene Struct. Expr.* **1988**, *950*, 395–402.
89. Schmid, P.; Lorenz, A.; Hameister, H.; Montenarh, M. Expression of p53 during mouse embryogenesis. *Development* **1991**, *113*, 857–865.
90. Ciaffardini, F.; Nicolai, S.; Caputo, M.; Canu, G.; Paccosi, E.; Costantino, M.; Frontini, M.; Balajee, A.; Proietti-De-Santis, L. The cockayne syndrome B protein is essential for neuronal differentiation and neuritogenesis. *Cell Death Dis.* **2014**, *5*, e1268–e1268.
91. Gjerstorff, M.F.; Harkness, L.; Kassem, M.; Frandsen, U.; Nielsen, O.; Lutterodt, M.; Møllgård, K.; Ditzel, H.J. Distinct GAGE and MAGE-A expression during early human development indicate specific roles in lineage differentiation. *Hum. Reprod.* **2008**, *23*, 2194–2201.
92. Wang, Y.; Herzig, G.; Molano, C.; Liu, A. Differential expression of the Tmem132 family genes in the developing mouse nervous system. *Gene Expr. Patterns* **2022**, *45*, 119257.
93. Liu, H.; Barnes, J.; Pedrosa, E.; Herman, N.S.; Salas, F.; Wang, P.; Zheng, D.; Lachman, H.M. Transcriptome analysis of neural progenitor cells derived from Lowe syndrome induced pluripotent stem cells: Identification of candidate genes for the neurodevelopmental and eye manifestations. *J. Neurodev. Disord.* **2020**, *12*, 14.
94. Johansson, P.A.; Brattås, P.L.; Douse, C.H.; Hsieh, P.; Adami, A.; Pontis, J.; Grassi, D.; Garza, R.; Sozzi, E.; Cataldo, R. A cis-acting structural variation at the ZNF558 locus controls a gene regulatory network in human brain development. *Cell Stem Cell* **2022**, *29*, 52–69.e58.
95. Yan, J.; Li, Q.; Mao, A.-P.; Hu, M.-M.; Shu, H.-B. TRIM4 modulates type I interferon induction and cellular antiviral response by targeting RIG-I for K63-linked ubiquitination. *J. Mol. Cell Biol.* **2014**, *6*, 154–163.
96. Han, D.; Wang, L.; Long, L.; Su, P.; Luo, D.; Zhang, H.; Li, Z.; Chen, B.; Zhao, W.; Zhang, N. The E3 Ligase TRIM4 Facilitates SET Ubiquitin-Mediated Degradation to Enhance ER-α Action in Breast Cancer. *Adv. Sci.* **2022**, *9*, 2201701.
97. Huang, Y.; Li, S.; Jia, Z.; Li, S.; He, W.; Zhou, C.; Zhang, R.; Xu, R.; Sun, B.; Ali, D.W. TRIM4 interacts with TRPM8 and regulates its channel function through K423-mediated ubiquitination. *J. Cell. Physiol.* **2021**, *236*, 2934–2949.
98. Zhang, H.; Guo, Y.; Gu, H.; Wei, X.; Ma, W.; Liu, D.; Yu, K.; Luo, W.; Ma, L.; Liu, Y. TRIM4 is associated with neural tube defects based on genome-wide DNA methylation analysis. *Clin. Epigenetics* **2019**, *11*, 17.
99. Wu, Z.; Zhu, X.; Yu, Q.; Xu, Y.; Wang, Y. Multisystem analyses of two Cockayne syndrome associated proteins CSA and CSB reveal shared and unique functions. *DNA Repair* **2019**, *83*, 102696.
100. Brooks, P. Blinded by the UV light: How the focus on transcription-coupled NER has distracted from understanding the mechanisms of Cockayne syndrome neurologic disease. *DNA Repair* **2013**, *12*, 656–671.

Disclaimer/Publisher's Note: The statements, opinions and data contained in all publications are solely those of the individual author(s) and contributor(s) and not of MDPI and/or the editor(s). MDPI and/or the editor(s) disclaim responsibility for any injury to people or property resulting from any ideas, methods, instructions or products referred to in the content.